

NACA RM A55F06



RESEARCH MEMORANDUM

ADDITIONAL COMPARISONS BETWEEN COMPUTED AND MEASURED
TRANSONIC DRAG-RISE COEFFICIENTS AT ZERO LIFT
FOR WING-BODY-TAIL CONFIGURATIONS

By George H. Holdaway

Ames Aeronautical Laboratory
Moffett Field, Calif.

CLASSIFICATION CHANGED

To UNCLASSIFIED

By authority of NACA Res obs effective
+ RN-128 Date June 24, 1958
AMT 8-12-58

CLASSIFIED DOCUMENT

This material contains information affecting the National Defense of the United States within the meaning of the espionage laws, Title 18, U.S.C., Secs. 793 and 794, the transmission or revelation of which in any manner to an unauthorized person is prohibited by law.

NATIONAL ADVISORY COMMITTEE FOR AERONAUTICS

WASHINGTON
August 15, 1955

AUG 17 1955
LANGLEY AERONAUTICAL LABORATORY
LANGLEY FIELD, VIRGINIA



NATIONAL ADVISORY COMMITTEE FOR AERONAUTICS

RESEARCH MEMORANDUM

ADDITIONAL COMPARISONS BETWEEN COMPUTED AND MEASURED

TRANSONIC DRAG-RISE COEFFICIENTS AT ZERO LIFT

FOR WING-BODY-TAIL CONFIGURATIONS

By George H. Holdaway

SUMMARY

Additional comparisons between computed wave-drag coefficients by the method of NACA RM A53H17 and measured values of drag rise from subsonic to supersonic speeds at zero lift are presented. The effect of an airfoil section modification was investigated for a wing plan form having 45° of sweepback and an aspect ratio of 3. Comparisons for triangular wings of aspect ratios 2, 3, and 4 indicate that the theory is valid for triangular wings with aspect ratios as large as 4 with airfoil sections as thick as 5 percent of the local chords.

INTRODUCTION

The computing method of reference 1 has been effectively used to estimate the effect of fuselage alterations on zero-lift drag-rise coefficients at transonic speeds for wing-body-tail combinations (refs. 2 and 3). This report makes further comparisons of the theoretical computing method with available experimental results, showing effects of wing plan-form changes, and the effect of an airfoil-section change on a wing of given plan form.

An indication of the effect of changes in wing plan form on the accuracy of the computing method was investigated by comparing measured drag-rise coefficients with calculated values for three triangular wings of aspect ratios 2, 3, and 4. The free-fall tests of these wings were with identical fuselage-tail combinations and covered a Mach number range of 0.84 to 1.12.

The effect of an airfoil-section change was investigated with a wing plan form having 45° of sweepback, an aspect ratio of 3, and a taper ratio of 0.4. The object of this portion of the investigation was to determine

████████████████████

if the computing method can be used to predict small changes in drag-rise coefficients due to small changes in the model area distribution. The wing airfoil-section change consisted of increasing the leading-edge radius and adding forward camber to improve the high lift characteristics at low speeds. These wings were tested (ref. 4) in the Ames 6- by 6-foot supersonic wind tunnel at high subsonic ($M = 0.6$ to 0.9) speeds and supersonic ($M = 1.2$ to 1.9) speeds.

SYMBOLS

A	aspect ratio
A_n	coefficients defining the magnitude of the harmonics of a Fourier sine series
C_{D_0}	zero-lift drag coefficient, $\frac{\text{drag at zero lift}}{qS_w}$
C_{D_0}'	zero-lift wave-drag coefficient, $\frac{\text{theoretical wave drag at zero lift}}{qS_w}$
ΔC_{D_0}	zero-lift drag-rise coefficient, $\frac{\text{zero-lift drag-rise above subsonic level}}{qS_w}$
c	local chord measured parallel to plane of symmetry
c'	local chord of the design airfoil sections
\bar{c}	mean aerodynamic chord of the total wing
l	fuselage or body length
M	free-stream Mach number
N	number of terms or harmonics used in the Fourier sine series
n	a harmonic of the Fourier sine series
q	free-stream dynamic pressure
S	projection of S_B on a plane perpendicular to x axis
S_B	areas formed by cutting configurations with planes perpendicular or oblique to the x axis
$S'(x)$	derivative or slope of S curves as a function of x
S_w	total wing area

- x distance measured from the nose of the model along the x axis
- x,y,z Cartesian coordinates as conventional body axes
- θ angle between the z axis and the intersection of the cutting planes X with the yz plane
(See ref. 1 for descriptive sketches and detailed definitions.)
- τ maximum wing thickness to chord ratio
- ϕ transformation of the length x to radians, $\arccos \left(1 - \frac{2x}{l} \right)$
- X a series of parallel cutting planes tangent to the Mach cone
(At $M = 1.0$ these planes are perpendicular to the x axis.)
- ψ angle in the xy plane between the intercept of the cutting planes X and the y axis, $\arctan \left(\sqrt{M^2 - 1} \cos \theta \right)$

MODELS AND TESTS

Triangular-Wing Models

The three triangular wings of aspect ratios of 2, 3, and 4 were all tested with the same fuselage-tail combination. The details of the models are given in figure 1 and table I. The equation in figure 1 for the fuselage radii up to station 139.4 is for a fineness-ratio-12 Sears-Haack body (minimum drag for prescribed volume and length). The radii for the remaining portion of the fuselage are given in table I.

The aspect-ratio-4 wing had airfoil sections (NACA 0005 streamwise) which were almost identical with the NACA 0005-63 sections used for the aspect-ratio-2 and -3 wings. Note further in table I that the wing areas were essentially equal (30 sq ft) with different mean aerodynamic chords of 5.19, 4.31, and 3.66 feet for the wings having aspect ratios of 2, 3, and 4, respectively.

The experimental investigations were conducted by the free-fall recoverable-model technique. The tests of these wings have been reported fully in references 5, 6, and 7. The tests covered the Mach number range from 0.86 to 1.12 with corresponding Reynolds numbers of about 1,500,000 to 3,000,000 per foot (8,200,000 to 16,500,000 for the mean aerodynamic chord of the wing with an aspect ratio of 4).

The estimated accuracy of the measurement of the drag coefficients for the triangular wings was $C_D = \pm 0.001$ which includes a 2-percent error in dynamic pressure, q , due to the possible error in Mach number of $M = \pm 0.01$.

Swept-Wing Models

Two swept-wing models were tested (ref. 4) to determine the effect of an airfoil section modification. The basic swept-wing model is shown in figure 2, with a sketch of the leading-edge modification which was tested on the second model. The local chords were increased approximately 2 percent by the modification. The fuselage, including the cut-off portion (fig. 2), is for a Sears-Haack type body having a fineness ratio of 12.5.

The basic wing had an aspect ratio of 3, a leading-edge sweep of 45° , a taper ratio of 0.4, and NACA 64A006 airfoil sections perpendicular to their own quarter-chord line. The wing plan-form area was 2.43 square feet and the mean aerodynamic chord was 0.956 feet.

The modified wing had a leading-edge sweep angle of 45.3° and modified airfoil sections as indicated by the ordinates listed in table II along with the corresponding ordinates of the basic wing. The change in wing profile consisted of an increased leading-edge radius with some camber added to the forward portion of the airfoil sections. The modified ordinates extended rearward to 40 percent of the local chords, c' , of the basic airfoil sections.

The tests and experimental procedures are reported in detail in reference 4 for these swept-wing models. The tests pertinent to this report were obtained in the 6- by 6-foot wind tunnel at a Reynolds number of 2,900,000 based on the mean aerodynamic chord of the basic wing. The subsonic tests ranged from $M = 0.6$ to 0.9 ; the supersonic tests from $M = 1.2$ to 1.9 .

RESULTS AND DISCUSSION

Triangular-Wing Models

Available experimental data on three wing plan forms having aspect ratios of 2, 3, and 4 enabled a comparison to be made with theoretical computations in order to further assess the range of applicability of the theory.

Computations.- The computations of wave-drag coefficients for these models were performed in the same manner, with the same cutting planes, as the examples given in reference 1. This discussion is concerned primarily with the effectiveness of the 24 harmonics of a Fourier sine series in satisfactorily representing the slopes of the area-distribution curves. Prior to obtaining the slopes of the area curves, the wing volumes for each cutting angle were checked to ensure that the volumes for each wing were equal to the integrated area of the wing area distributions shown in figure 3.

The degree of convergence of the Fourier coefficients in the summation $\sum_{n=1}^N nA_n^2$ used in the calculation of the theoretical drag coefficients was checked as was done in reference 8, and the results are shown in figure 4 for the three triangular wings. Data points are shown for the five cutting angles in the xy plane of $\psi = 0^\circ, 8.1^\circ, 11.4^\circ, 17.8^\circ,$ and 28.7° . As discussed in reference 1, the computation of the drag coefficients at $M = 1.00$ used only the final summation ($N = 24$) for $\psi = 0^\circ$, but the $M = 1.14$ computation, for example, used all five final summations. For each wing the $\psi = 0^\circ$ ($M = 1.00$) curve shows a lack of convergence, and perhaps a larger number of terms should be used, although this would tend to increase the theoretical drag and the disagreement normally obtained at a Mach number of 1.00 between theory and experiment.

A more direct evaluation of the effectiveness of the 24 terms of the Fourier series, in representing the original machine-computed slopes of the area-distribution curves, was obtained by checking the slope curves by utilizing the equation:

$$S'(x) = \sum_{n=1}^{24} A_n \sin n\psi$$

where the values of A_n are those computed in determining the wave drag. An example of this procedure is shown in figure 5, where the slope curves for the aspect-ratio-3 wing were satisfactorily checked. As might be expected from the discussion on convergence, the sharp peak of the $\psi = 0^\circ$ ($M = 1.00$) curve is not matched by the 24-term solution.

The results of the theoretical calculations for the triangular-wing models are shown in figure 6, and as would be expected the higher aspect ratio wings also have the higher wave drag.

Comparison of theory with experiment.— The results of the experiments and computations for the three triangular-wing models are compared in figure 7. For the aspect-ratio-2 and -3 wings (figs. 7(a) and 7(b)), the computations predicted the drag-rise coefficients at supersonic speeds exceptionally well. For these two wings the differences between the calculated and experimental values are generally less than 5 percent, and actually are less than the experimental scatter.

The comparison for the aspect-ratio-4 wing is made in figure 7(c). The data points indicated by circles were obtained during oscillating flight and were used in the original comparison with theory for this wing (ref. 1). Subsequent experiments and detailed inspection of photographs of the model in flight proved that the original data were not for a clean configuration. The photographs showed that the rear hanger used to support the model had not retracted (see fig. 8). The new subsonic drag coefficients are now in agreement with values for the aspect-ratio-2 and -3

wings, and the new comparison between experiment and theory is consistent with the other tests of reference 1 in that the theory is somewhat low at supersonic speeds. In this case the maximum deviation of the theory occurs at $M = 1.12$ and is about 12 percent, which is well within the 20-percent value stated in reference 1. It is interesting to note that, although reference 9 suggests a value of $A(\tau)^{1/3}$ of unity as the limit of applicability of the area rule (ref. 10) for rectangular wings, this triangular wing has a value of $A(\tau)^{1/3}$ equal to 1.47 and the theory is still applicable.

Comparison of experimental results.— Of interest, although of secondary importance to this report, is a comparison between the experimental results for the wings of different aspect ratios (fig. 9). As was mentioned previously, all three models have similar drag coefficients at subsonic speeds. The apparent progressive increase in the drag-divergence Mach number with increasing aspect ratio would not be generally expected due to the decrease in leading-edge-sweep angle with increased aspect ratio. However, for most swept wings without bodies, the critical pressure coefficient occurs first on the root airfoil section (ref. 11). Mounting swept wings on a body of finite, but not infinite, radius decreases these distortion velocities (e.g., ref. 12). In the case of this report, the wing-body interference might cause the increase in drag-divergence Mach number with increased aspect ratio. Further analysis and investigation are required before any definite conclusions are drawn.

Swept-Wing Models

This section of the discussion is concerned with the evaluation of the computing method for estimating drag changes due to relatively minor profile changes. For both the basic and modified airfoil sections the rounded noses (fig. 2) result in area distribution curves which have infinite slopes when the cutting planes are parallel to the wing leading edge. Thus for this wing plan form and Mach numbers equal to $\sqrt{2}$ or greater, linear theory, on which the computing method is based, is basically unsuited for computing the effect of small changes in leading-edge radius, because a rigorous application of the theory will give absurd answers (infinite wave drags). However, previous experience with subsonic leading edges has shown that computations limited to 24 harmonics smooth out slight discontinuities in the area-distribution curve. Thus, it would be of interest to apply the computing method for the entire range of test Mach numbers and determine the shape of the sharpened airfoil sections defined by the 24-term solution at the higher Mach numbers. The computations and comparisons above a Mach number of $\sqrt{2}$ would strictly apply only for the sharpened (both basic and modified) airfoil sections.

Computations.— Details of these computations are somewhat different than those of reference 1; therefore, some explanation of the procedures used is desirable. A Mach number of 1.5 was selected for the example computation.

The computations were made from the area distributions determined for the low-speed model (ref. 4) which will be referred to as the "full-scale" model in this report. Presented in figure 10 are the full-scale-model area distributions used in the computation of the wave-drag coefficients for a Mach number of 1.5. These area distributions were determined for cutting planes in only one quadrant of θ because of the symmetry of the model, and thus only five cuts were made at equal 22.5° increments of θ . The corresponding intercept angles (ψ) in the xy plane were 0° , 23.2° , 38.4° , 46.0° , and 48.2° . The $\psi = 0^\circ$ cut was also used to compute the wave drag at $M = 1.0$, and the cutting angles of $\psi = 0^\circ$, 23.2° , and 38.4° were also used to estimate the wave drag at $M = 1.28$. To estimate the wave drag at a Mach number of 1.9 an additional cut was made for $\psi = 58.25^\circ$ and this area curve (fig. 11) was used with the curves obtained for the $M = 1.5$ computation converted to new angles of θ .

The degree of convergence of the summation $\sum_{n=1}^N nA_n^2$ is shown in

figure 12 for the basic and modified wings for the five cutting angles for Mach number 1.5. Reasonable convergence of the series for the 24 terms is indicated for the three smaller cutting angles, and the solution probably is valid (see ref. 8). As was expected, particularly for the modified wing, the series for the $\psi = 46^\circ$ and $\psi = 48.2^\circ$ cuts (supersonic leading edges) show rather slow convergence (fig. 12(b)) and indicate that the solution is questionable.

The validity of the computations was investigated by making check solutions of the slope curves of the area distributions. As before, the check points were computed from the A_n values derived in the drag computations. The limiting of the solution to 24 terms resulted in little smoothing of the $S'(x)$ curves for the Mach number 1.00 cuts for these wings (fig. 13(a)). On the other hand, 24 terms did not define the sharp peaks of the $\psi = 46^\circ$ cuts for both wings (fig. 13(b)). Thus the 24-term solutions for Mach numbers greater than the $\sqrt{2}$ are not for rounded airfoil sections, but for wings with sharp leading edges of the type shown in figure 14 for $\psi = 46^\circ$. These nose fairings are required primarily for cuts near the sweep angle of the wing leading edge, and the effects of these fairings (slight volume change) are relatively small at other cutting angles.

The values of $\sum_{n=1}^{24} nA_n^2$ were plotted against θ as shown in figure

15 and the areas under the curves were integrated to obtain the wave-drag coefficients:

$$C_{D_0} = \frac{1}{9} \times 10^{-4} \int_0^{\pi/2} \sum_{n=1}^{24} nA_n^2 d\theta$$

for the two wings. This figure illustrates the large peak values of the summation which occur when the cutting planes are parallel to the wing leading edge. Slight rounding of the peaks produces very little change in the integrated area. In spite of these difficulties in the $M = 1.5$ computation, at each value of θ the summation for the modified wing (with a sharp leading edge, fig. 14) is greater than that for the basic wing and there is no question as to the lower theoretical drag of the basic wing. For higher Mach numbers such as the $M = 1.9$ computation, the fairing toward the peaks covers a smaller range of θ .

Although the sting-mounted models did not have complete Sears-Haack bodies (fig. 10(a)), in the computations they were initially considered to have such; then the forebody wave-drag coefficients were estimated by subtracting a correction of 0.0004. This correction was determined from the difference between the computed wave-drag coefficients for the complete fuselage and the computed forebody coefficients for the cut-off fuselage.

$$C_{D_0}'(\text{Sears-Haack body}) - C_{D_0}'(\text{cut-off Sears-Haack forebody}) \\ = 0.0036 - 0.0032$$

The wave-drag coefficient of the cut-off Sears-Haack body was computed as follows: The area curve of the cut-off body was divided into two parts by plotting the area distribution of a von Kármán ogive with its infinite cylinder having a cross-sectional area equal to the base area of the cut-off Sears-Haack body. To the wave-drag coefficient of the von Kármán ogive was added a computed (method of ref. 1) coefficient for the second part of the area-distribution curve for the cut-off Sears-Haack body. It was necessary to alter slightly this second or remaining area distribution to produce zero slope at the point of cut-off. This approximation was felt to be justified since the total correction was small.

Comparison of theory with experiment.— Figure 16 presents the experimental zero-lift drag coefficients from wind-tunnel data for the swept-wing models with the computed wave-drag coefficients added to the subsonic level of the experimental data. The coefficients are all forebody values and, as described previously, the theoretical values (based only on area distributions, no evaluation of the slight camber) were computed at Mach numbers of 1.00, 1.28, 1.50, and 1.90. The computations for $M = 1.50$ and $M = 1.90$ are for the sharp-nose sections of figure 14. The difference between computed and experimental values of the drag-rise coefficients for the basic wing were generally less than 20 percent of the experimental values for the supersonic Mach numbers of 1.2 to 1.9. Comparable agreement for the modified wing occurred from Mach numbers of 1.2 to 1.5.

The difference in drag-rise coefficients between the basic and modified wings as indicated by theory (sharp-nose sections) and experiment is influenced by the difference in camber. The effect of the slight camber was estimated, using an equivalent flap and the procedures of reference 13 (applicable to wings with supersonic leading edges). Mach numbers of 1.5 and 1.9 were selected to illustrate the added drag rise of the modified

wing over the basic wing as shown in figure 17. The agreement between theory and experiment at $M = 1.5$ is better than might be expected with the assumptions involved. At a Mach number of 1.9 the theory underestimated the increase in drag-rise coefficient due to the modification, but the theory did show an increase and the percentage increase is very similar to the percentage increase in the experimental values. This graph also illustrates the unresolved problem that the experimental drag coefficients increased from $M = 1.5$ to 1.9, whereas all components of the theoretical values, including the effect of camber, decreased.

CONCLUDING REMARKS

A further evaluation has been made of the theoretical computing method of reference 1 for predicting zero-lift wave-drag coefficients. The cases examined were three triangular-wing models of aspect ratios 2, 3, and 4, and a basic and a modified airfoil section on a wing plan form having 45° of sweepback.

The computing method is apparently valid for triangular wings with aspect ratios as large as 4 with an airfoil section 5 percent thick. For the triangular-wing models tested, 24 harmonics of a Fourier sine series were adequate to represent the slope curves of the model area distributions and hence to compute the wave-drag coefficients. The errors of prediction in each case were considerably less than the 20-percent value stated in reference 1.

The basic theory is inapplicable to area distributions which have extreme slopes or an extreme discontinuity in slope, both of which occurred for the swept-wing models at Mach numbers above 1.4. The computing method smoothed the area distributions and qualitatively predicted at all Mach numbers the increase in wave drag for the relatively minor profile change. For supersonic speeds up to $M = 1.5$, the quantitative predictions of the drag-rise coefficients for the swept-wing models were again within 20 percent of the experimental values.

Ames Aeronautical Laboratory
National Advisory Committee for Aeronautics
Moffett Field, Calif., June 6, 1955

REFERENCES

1. Holdaway, George H.: Comparison of Theoretical and Experimental Zero-Lift Drag-Rise Characteristics of Wing-Body-Tail Combinations Near the Speed of Sound. NACA RM A53HL7, 1953.

2. Carmel, Melvin M.: An Experimental Transonic Investigation of a 45° Sweptback Wing-Body Combination With Several Types of Body Indentation With Theoretical Comparisons Included. NACA RM L54IO7a, 1954.
3. Holdaway, George H.: An Experimental Investigation of Reduction in Transonic Drag Rise at Zero Lift by the Addition of Volume to the Fuselage of a Wing-Body-Tail Configuration and a Comparison With Theory. NACA RM A54F22, 1954.
4. Graham, David, and Evans, William T.: Investigation of the Effects of an Airfoil Section Modification on the Aerodynamic Characteristics at Subsonic and Supersonic Speeds of a Thin Swept Wing of Aspect Ratio 3 in Combination With a Body. NACA RM A55D11, 1955.
5. Bright, Loren G.: A Flight Investigation at Transonic Speeds of a Model Having a Triangular Wing of Aspect Ratio 4. NACA RM A54L27, 1955.
6. White, Maurice D.: A Flight Investigation at Transonic Speeds of a Model Having a Triangular Wing of Aspect Ratio 3. NACA RM A55D18, 1955.
7. White, Maurice D.: A Flight Investigation at Transonic Speeds of a Model Having a Triangular Wing of Aspect Ratio 2. NACA RM A55F21, 1955.
8. Alksne, Alberta: A Comparison of Two Methods for Computing the Wave Drag of Wing-Body Combinations. NACA RM A55A06a, 1955.
9. Spreiter, John R.: On the Range of Applicability of the Transonic Area Rule. NACA RM A54F28, 1954.
10. Whitcomb, Richard T.: A Study of the Zero-Lift Drag-Rise Characteristics of Wing-Body Combinations Near the Speed of Sound. NACA RM L52H08, 1952.
11. Kuchemann, D.: Design of Wing Junction, Fuselage and Nacelles to Obtain the Full Benefit of Sweptback Wings at High Mach Number. R.A.E. Rep. No. Aero. 2219, British, 1947.
12. Byrd, Paul F.: Theoretical Pressure Distributions for Some Slender Wing-Body Combinations at Zero Lift. NACA RM A54J07, 1955.
13. Frick, Charles W., Jr.: Application of the Linearized Theory of Supersonic Flow to the Estimation of Control Surface Characteristics. NACA TN 1554, 1948.

TABLE I.- DIMENSIONS OF TRIANGULAR WING MODELS

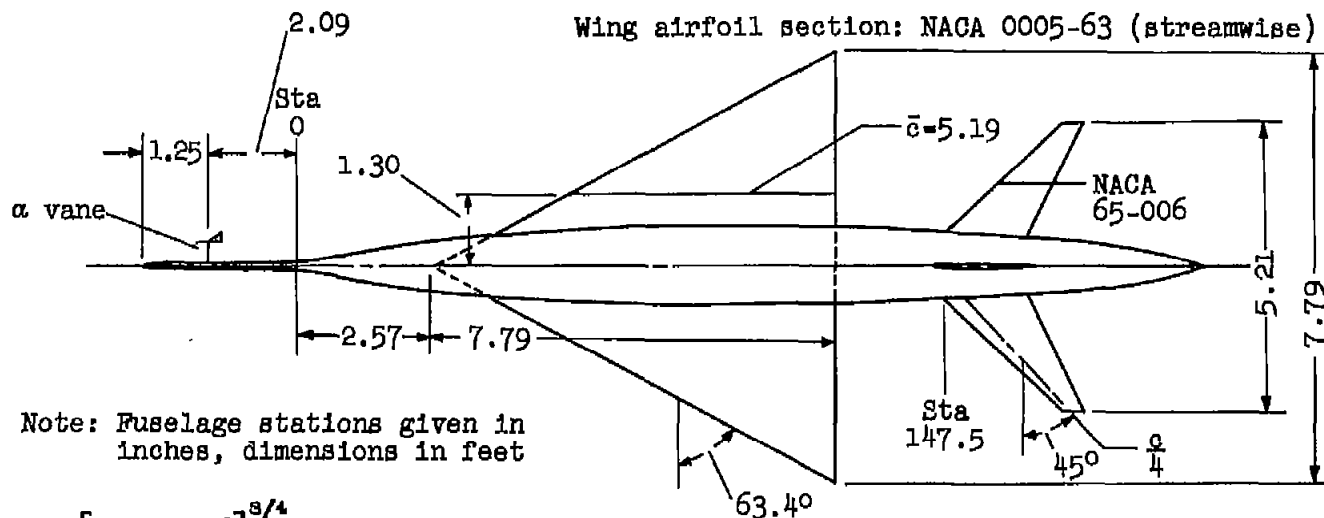
Wings			
Aspect ratio	2	3	4
Area, sq ft	30.3	31.4	30.0
Mean aerodynamic chord, ft	5.19	4.31	3.66
Airfoil sections, NACA streamwise	0005-63	0005-63	0005
Fuselage			
Fineness ratio			12.4
Maximum diameter, in.			17.0
Nose boom diameter, in.			1.50
Fuselage radii at stations behind the theoretical ordinates			
	<u>Fuselage station</u>	<u>Inches</u>	
	140.0	7.23	
	150.0	7.10	
	160.0	6.60	
	165.0	6.34	
	189.6	5.10	
	195.6	4.50	
	201.6	3.20	
	204.6	2.30	
	210.5	0	
Horizontal-tail surfaces			
Area, sq ft			6.0
Aspect ratio			4.5
Taper ratio			0.2
Airfoil section, streamwise		NACA	65-006
Sweep of streamwise 0.25 chord, deg			45.0
Vertical-tail surfaces			
Area, sq ft			3.1
Aspect ratio			5.1
Taper ratio			0.22
Airfoil section, perpendicular to the line of their own 0.25 chords ($c^1/4$)		NACA	65-009
Sweep of $c^1/4$ line, deg			45.0

TABLE II.- COORDINATES OF THE AIRFOIL SECTIONS USED FOR THE 45° SWEEP WING [All coordinates are referred to the chord of the NACA 64A006 section, and are in terms of percent of that chord. Asterisks indicate ordinates that are identical to those of the NACA 64A006 section. Sections are perpendicular to the 39.45° sweep line ($c'/4$).]

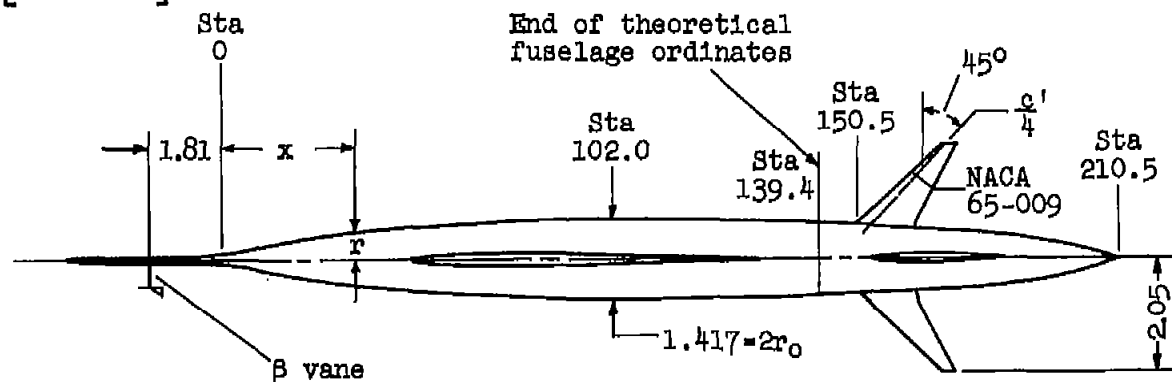
Station	Basic sections NACA 64A006 ordinate	Ordinates of modified sections	
		Upper surface	Lower surface
-1.50		-1.38	-1.38
-1.25		-0.60	-2.065
-1.00		-0.34	-2.315
-0.75		-0.145	-2.49
-0.25		0.16	-2.75
0.00	0	0.29	-2.855
0.25		0.395	-2.955
0.50	.485	0.49	-3.04
0.75	.585	*	-3.10
1.25	.739		-3.22
2.5	1.016		-3.405
5.0	1.399		-3.615
7.5	1.684		-3.70
10	1.919		-3.74
15	2.283		-3.655
20	2.557		-3.445
25	2.757		-3.245
30	2.896		-3.105
35	2.977		-3.025
40	2.999		-3.000
45	2.945		*
50	2.825		
55	2.653		
60	2.438		
65	2.188		
70	1.907		
75	1.602		
80	1.285		
85	.967		
90	.649		
95	.331		
100	.013		

Modified section:
 Leading-edge radius = 1.19
 Center of leading-edge circle $x = -0.31$
 $y = -1.33$

Basic section:
 Leading-edge radius = 0.24



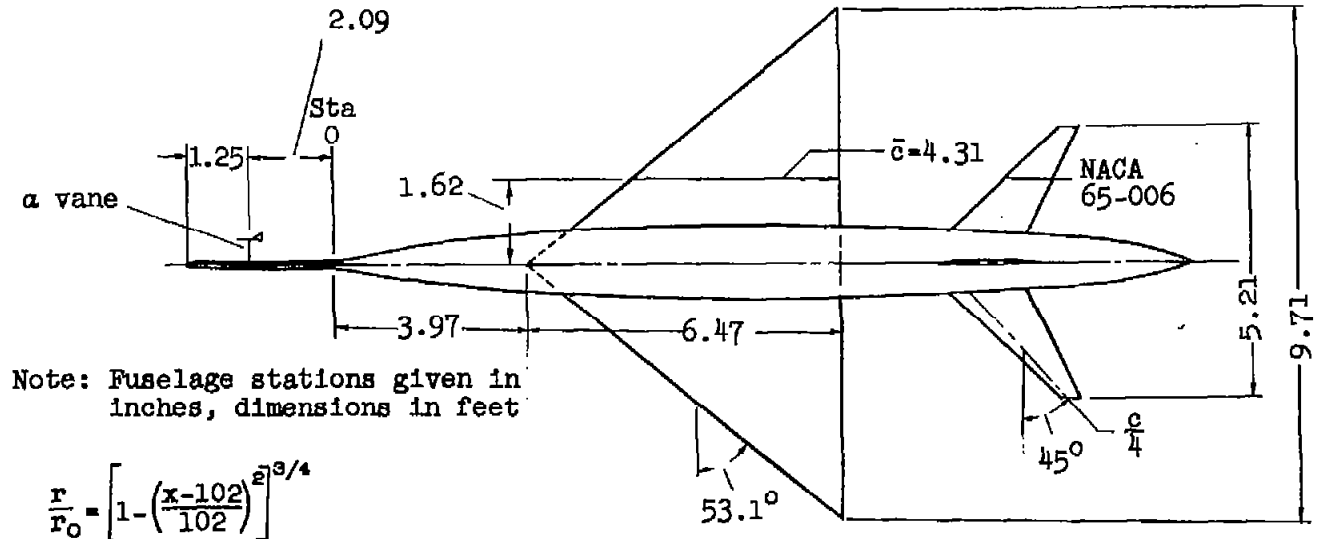
$$\frac{r}{r_0} = \left[1 - \left(\frac{x-102}{102} \right)^2 \right]^{3/4}$$



(a) Aspect-ratio-2 wing.

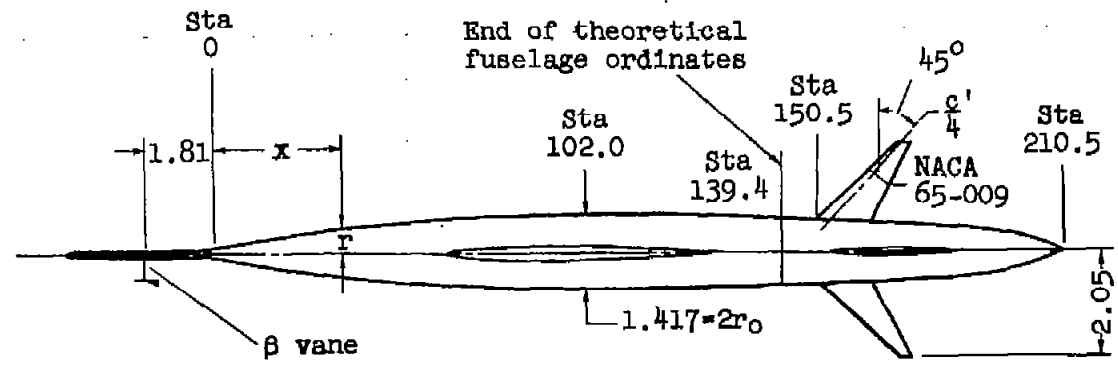
Figure 1.- Models with triangular wings. All three models are identical except for the wing.

Wing airfoil section: NACA 0005-63 (streamwise)



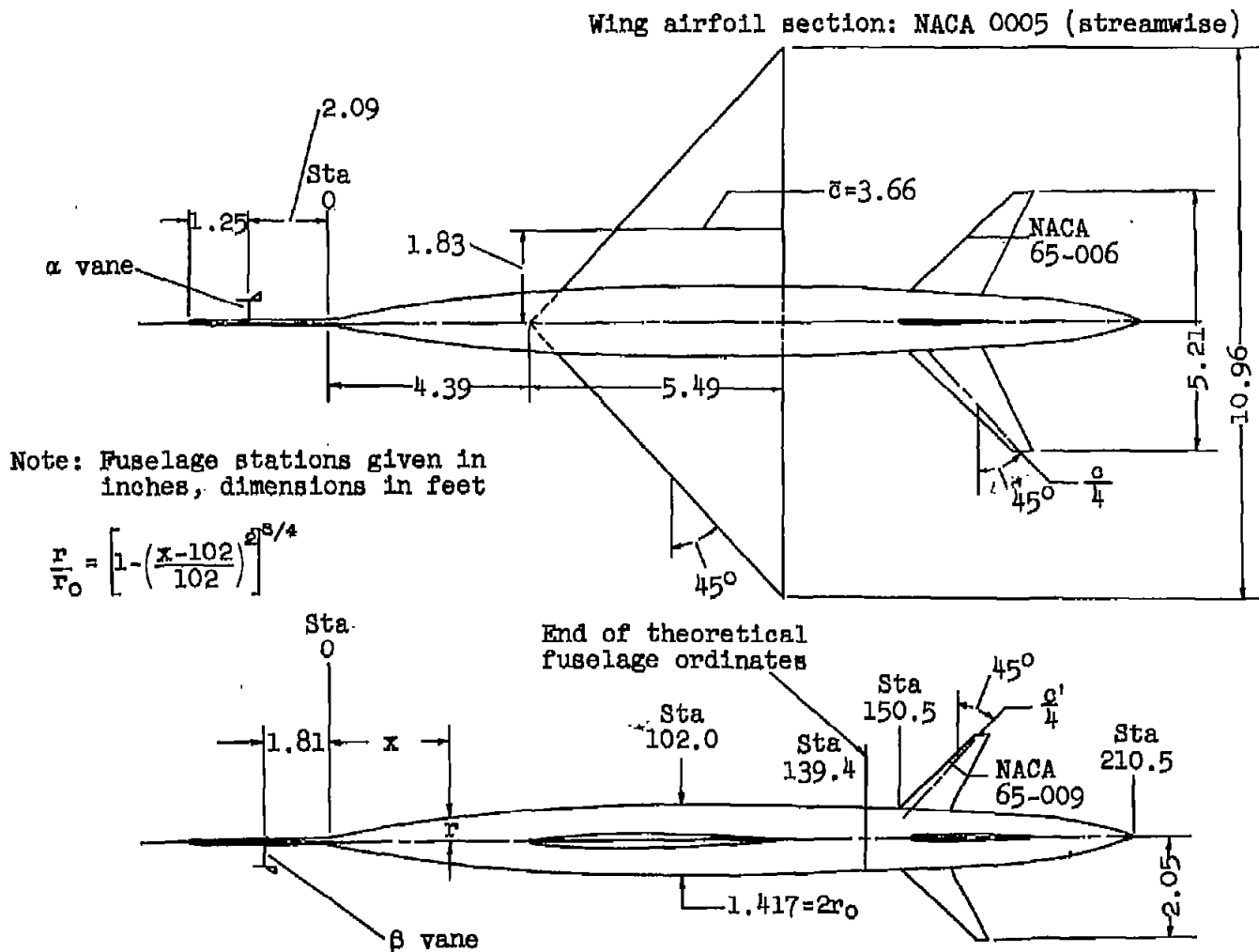
Note: Fuselage stations given in inches, dimensions in feet

$$\frac{r}{r_0} = \left[1 - \left(\frac{x-102}{102} \right)^2 \right]^{3/4}$$



(b) Aspect-ratio-3 wing.

Figure 1.- Continued.



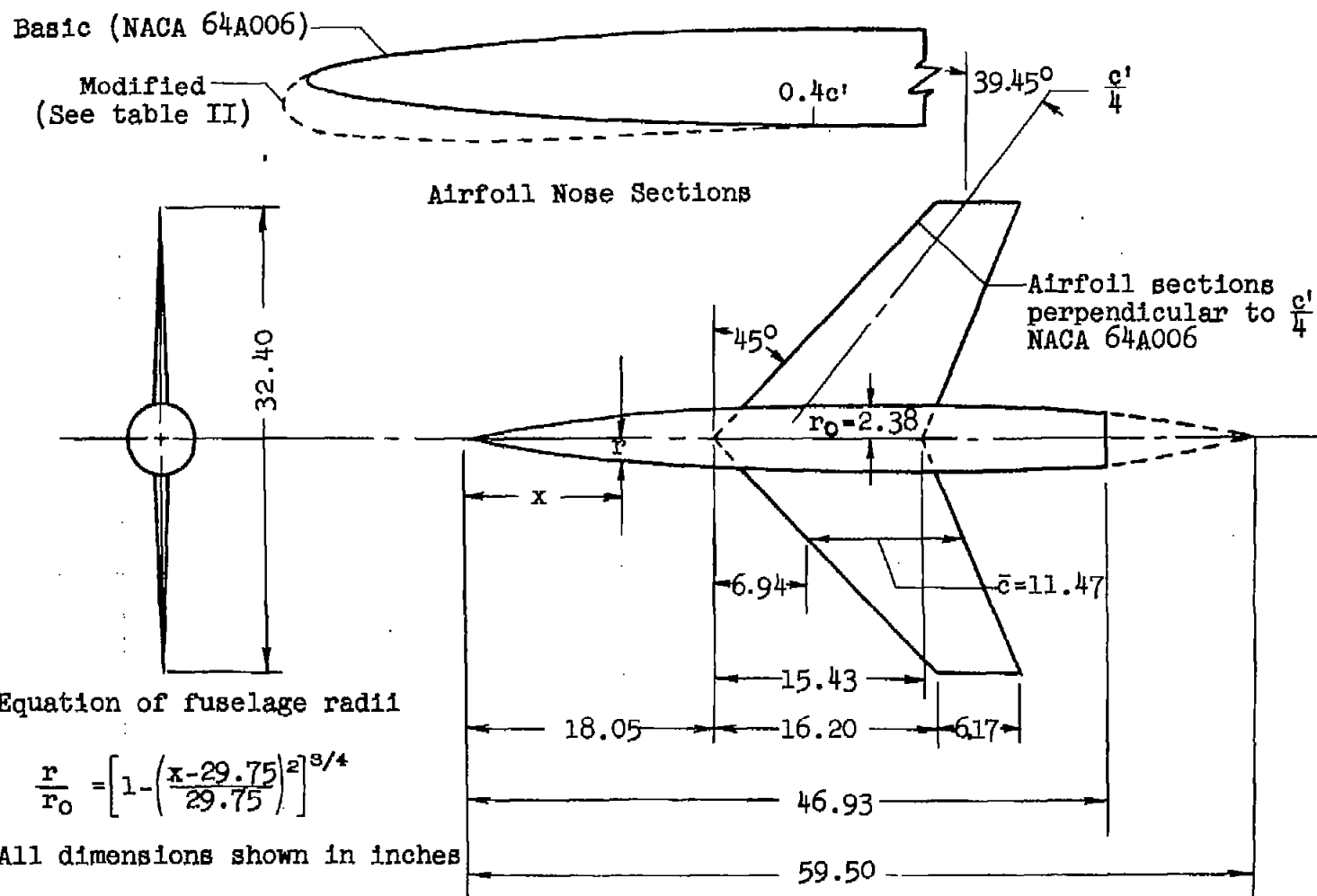


Figure 2.- Swept-wing model.

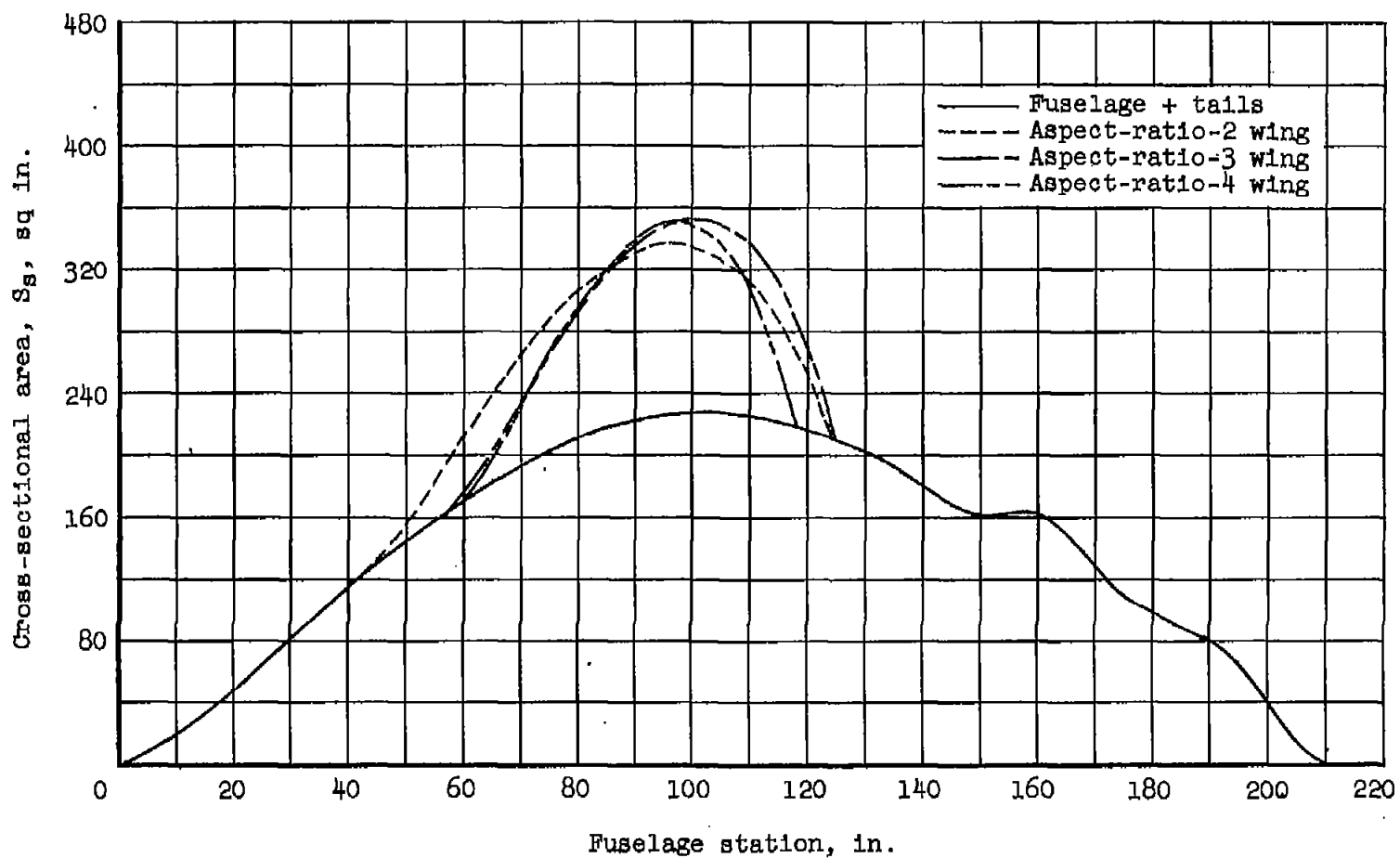
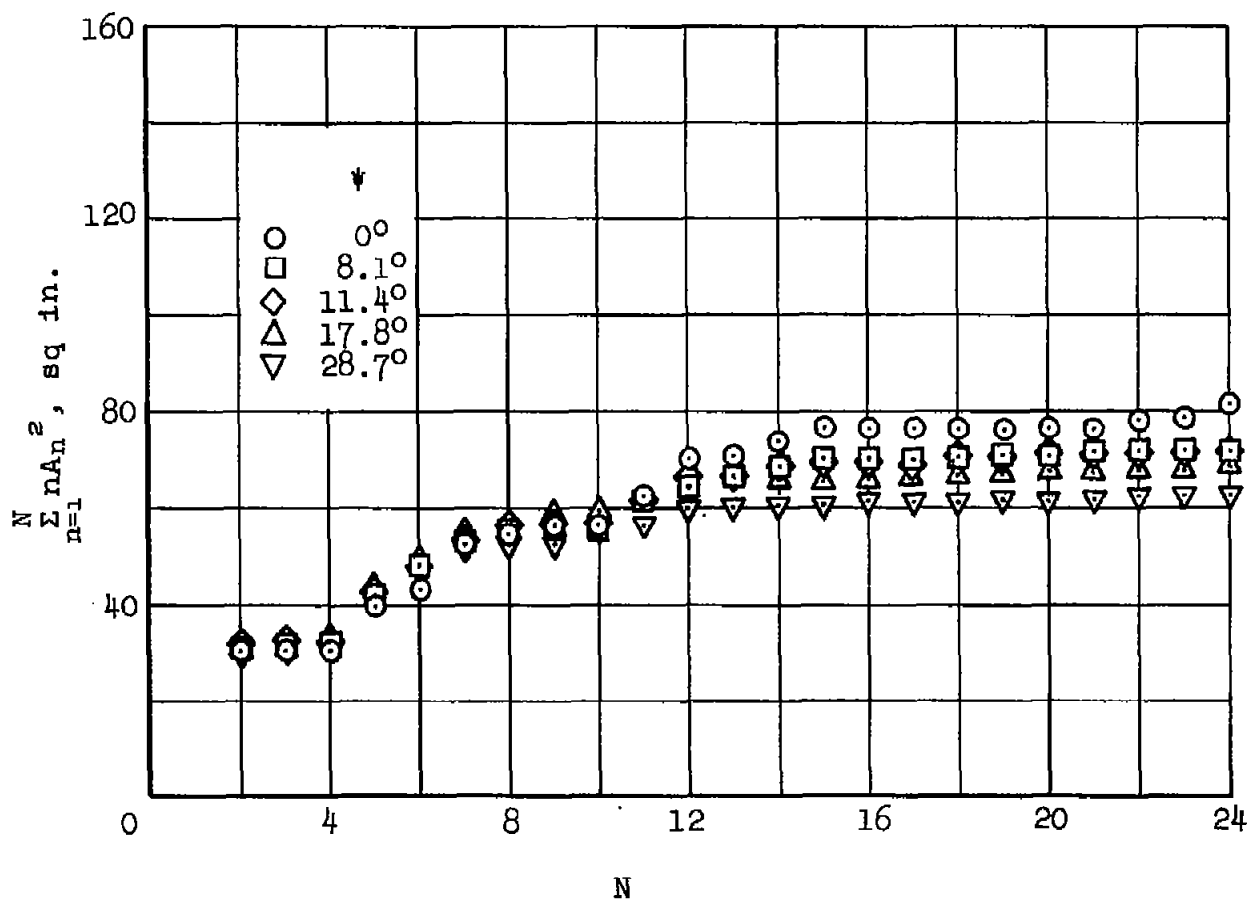
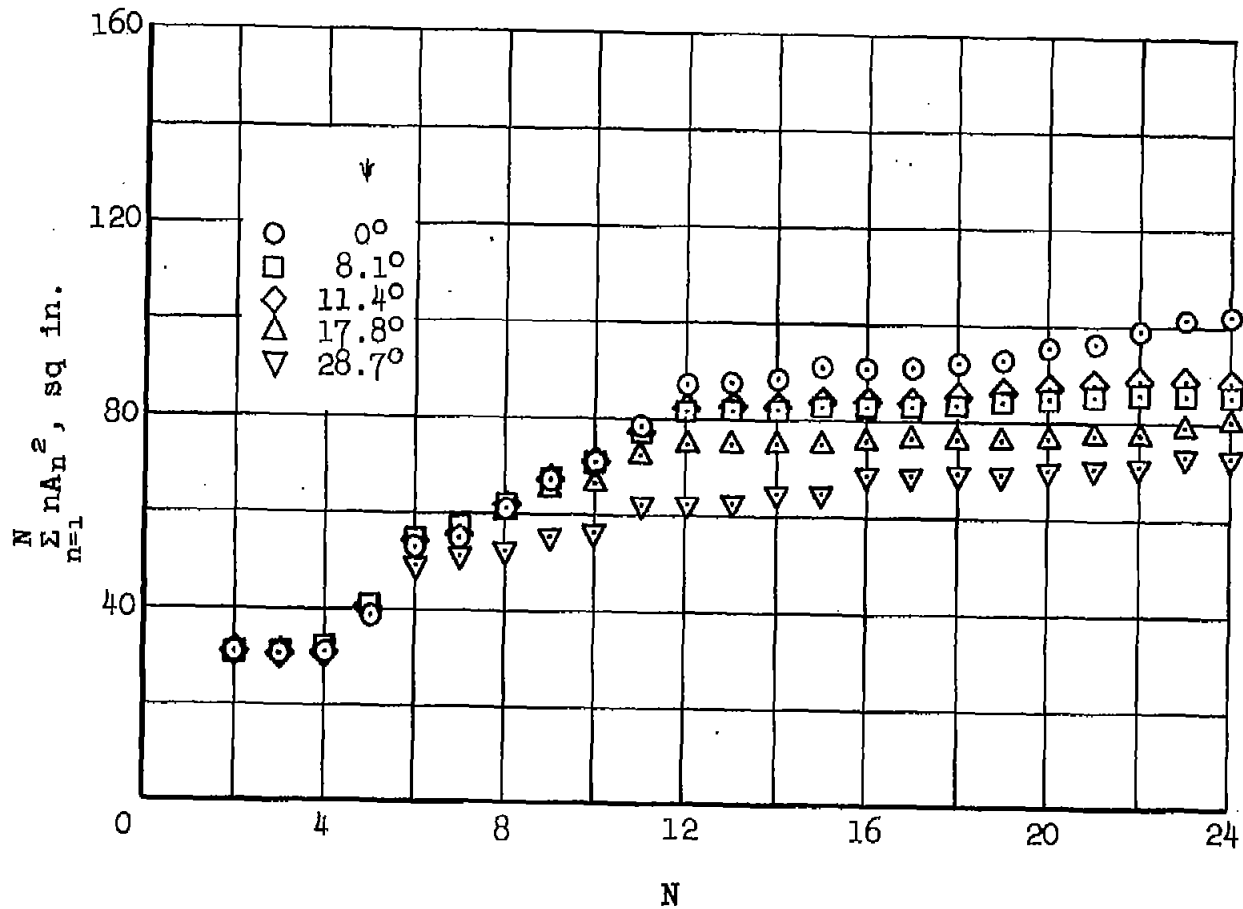


Figure 3.- Cross-sectional area distributions for the triangular-wing models.



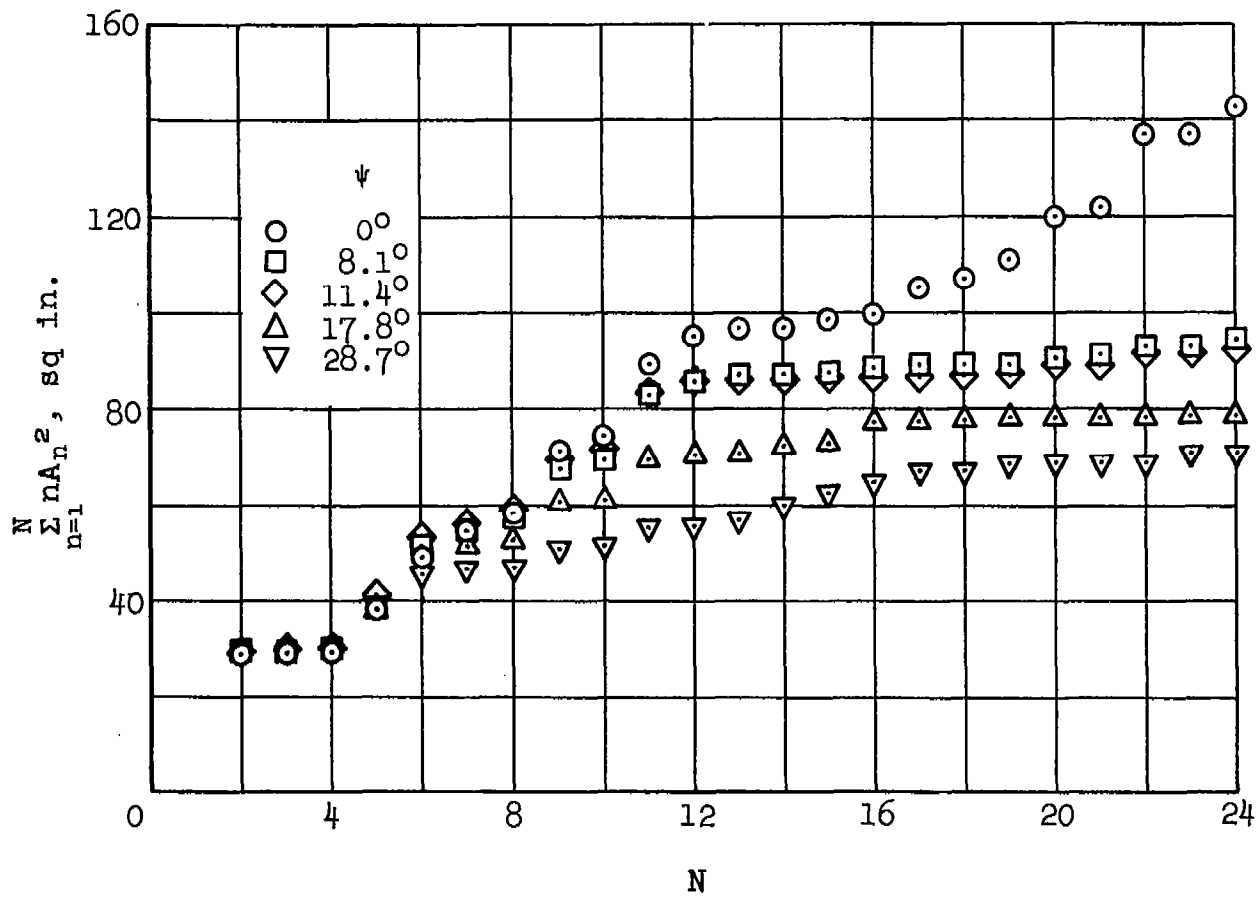
(a) Aspect-ratio-2 wing.

Figure 4.- Variation of $\sum_{n=1}^N n A_n^2$ with N for the triangular-wing models for five cutting angles.



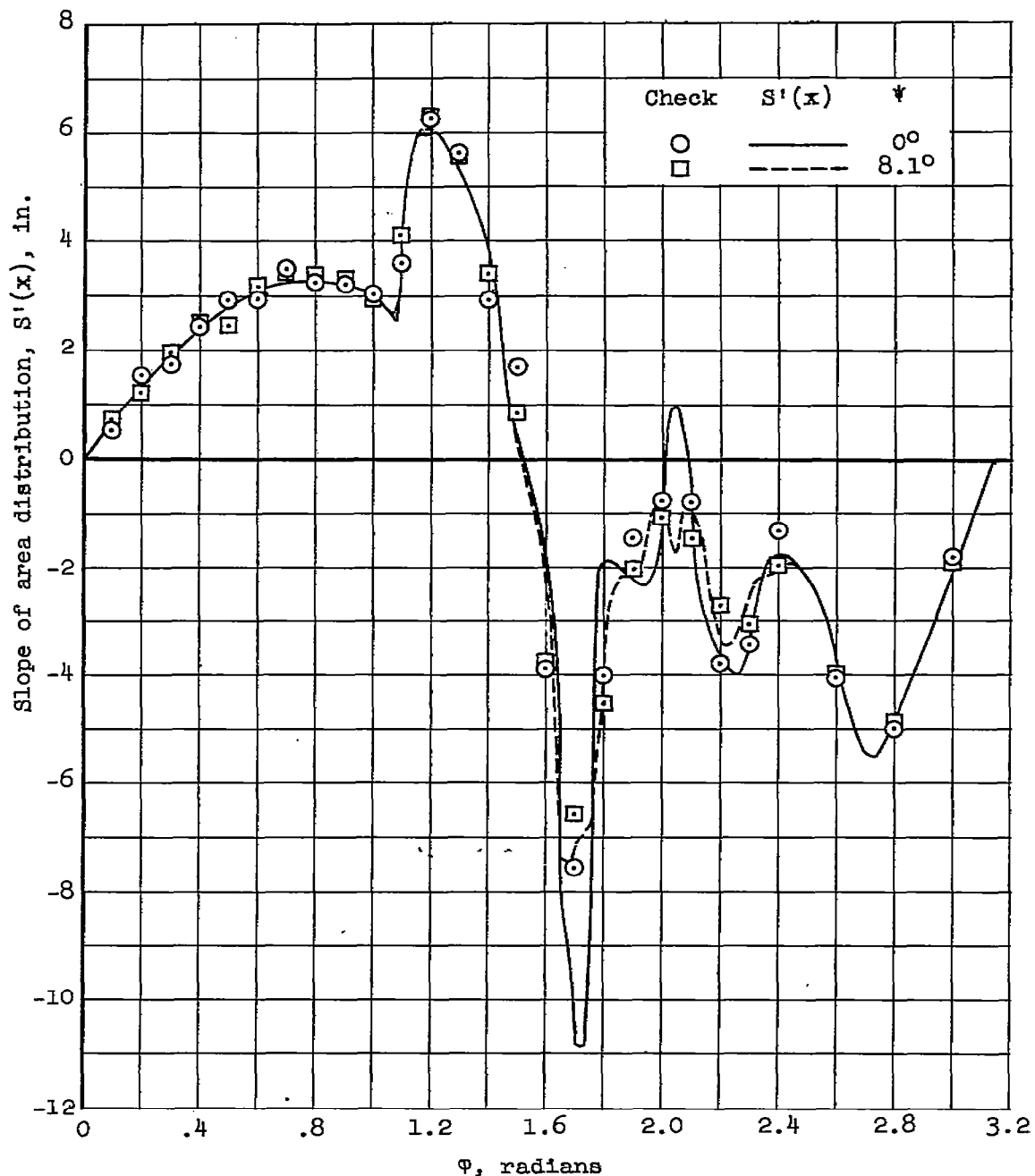
(b) Aspect-ratio-3 wing.

Figure 4.- Continued.



(c) Aspect-ratio-4 wing.

Figure 4.- Concluded.



(a) Cutting planes for $\psi = 0^\circ$ and 8.1° .

Figure 5.- Check of the effectiveness of the solution of the Fourier sine series (24 terms) to represent the curves of $S'(x)$ used in the wave-drag calculations for the aspect-ratio-3 triangular wing.

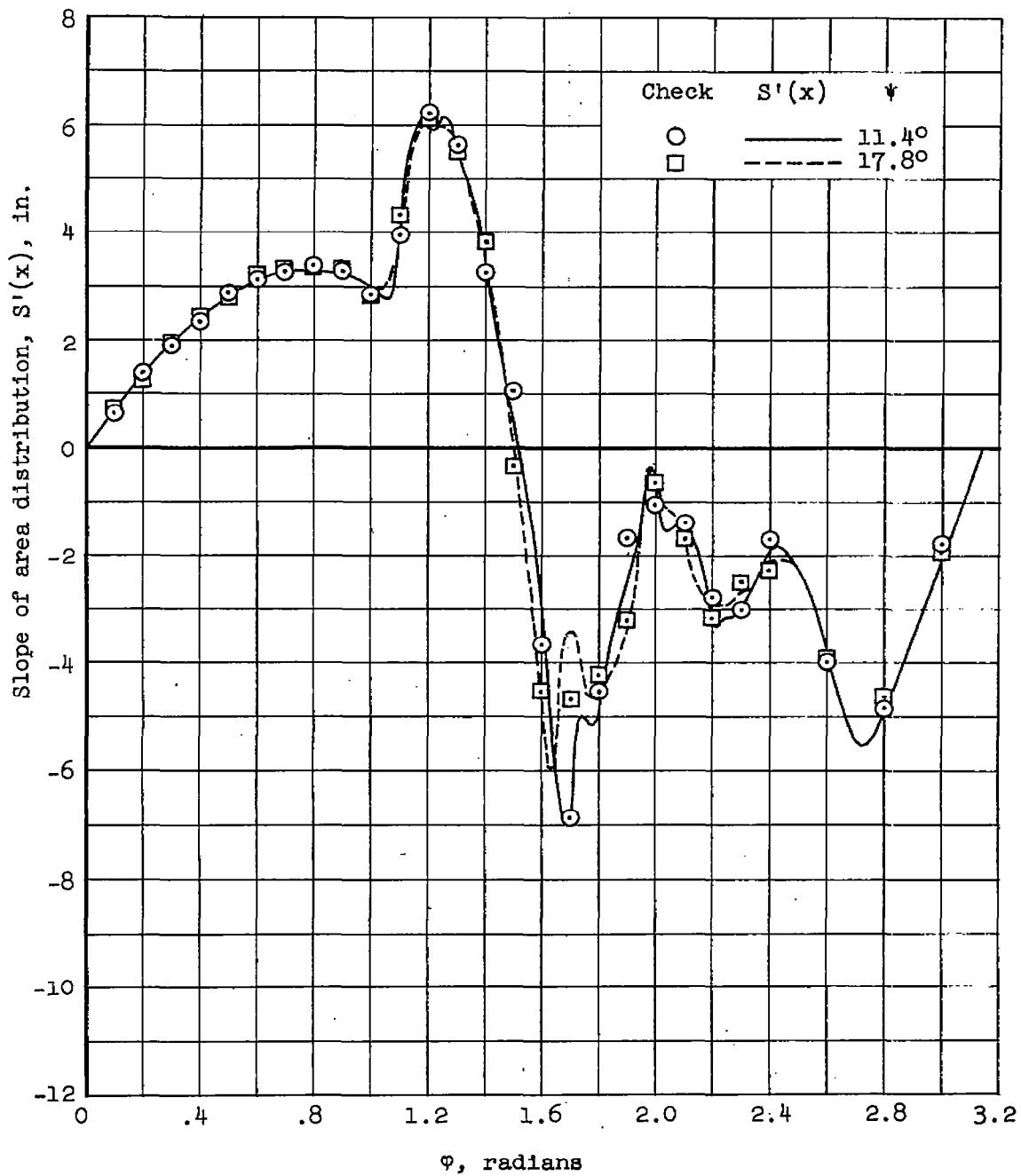
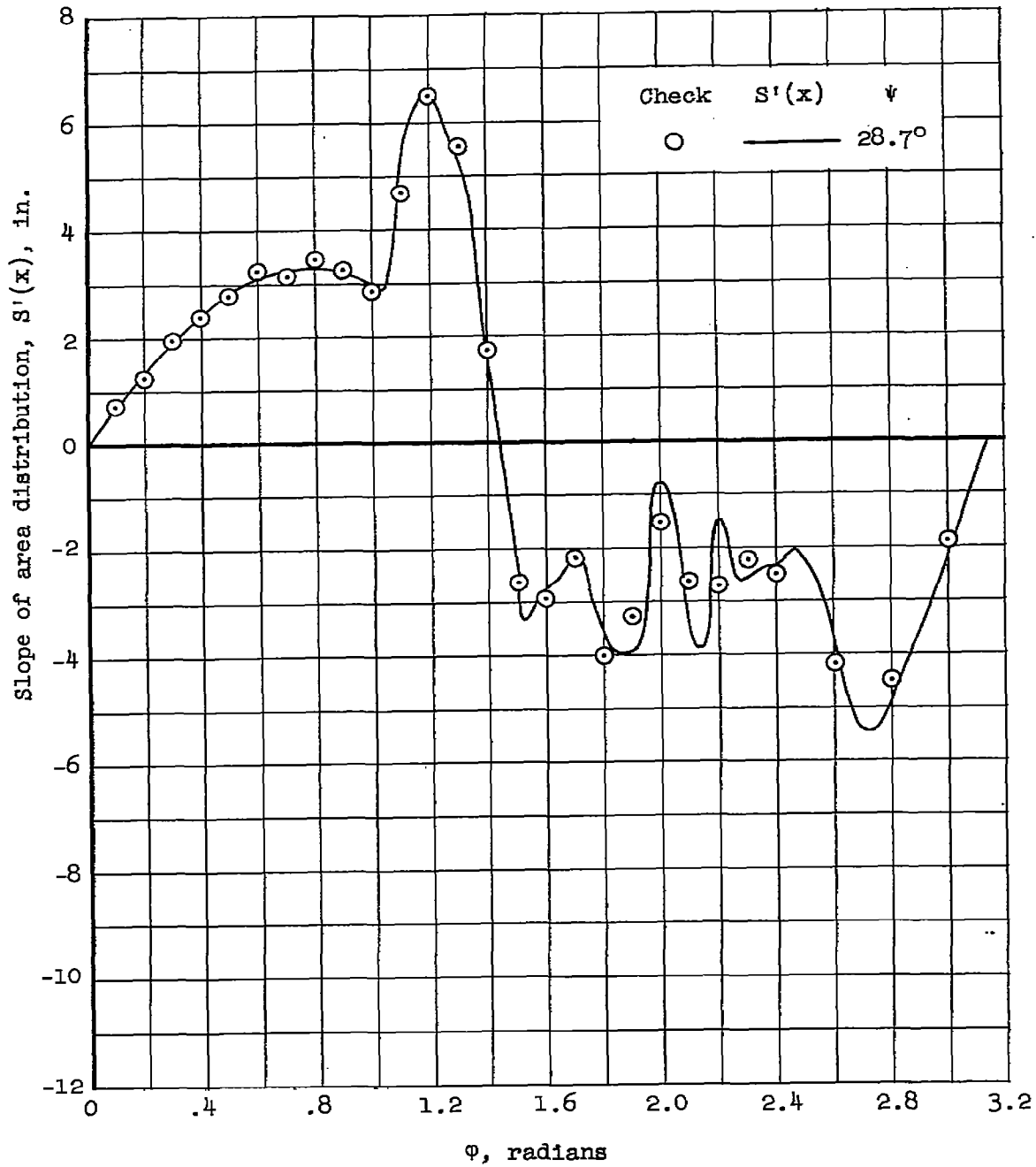
(b) Cutting planes for $\psi = 11.4^\circ$ and 17.8° .

Figure 5.- Continued.



(c) Cutting planes for $\psi=28.7^\circ$.

Figure 5.- Concluded.

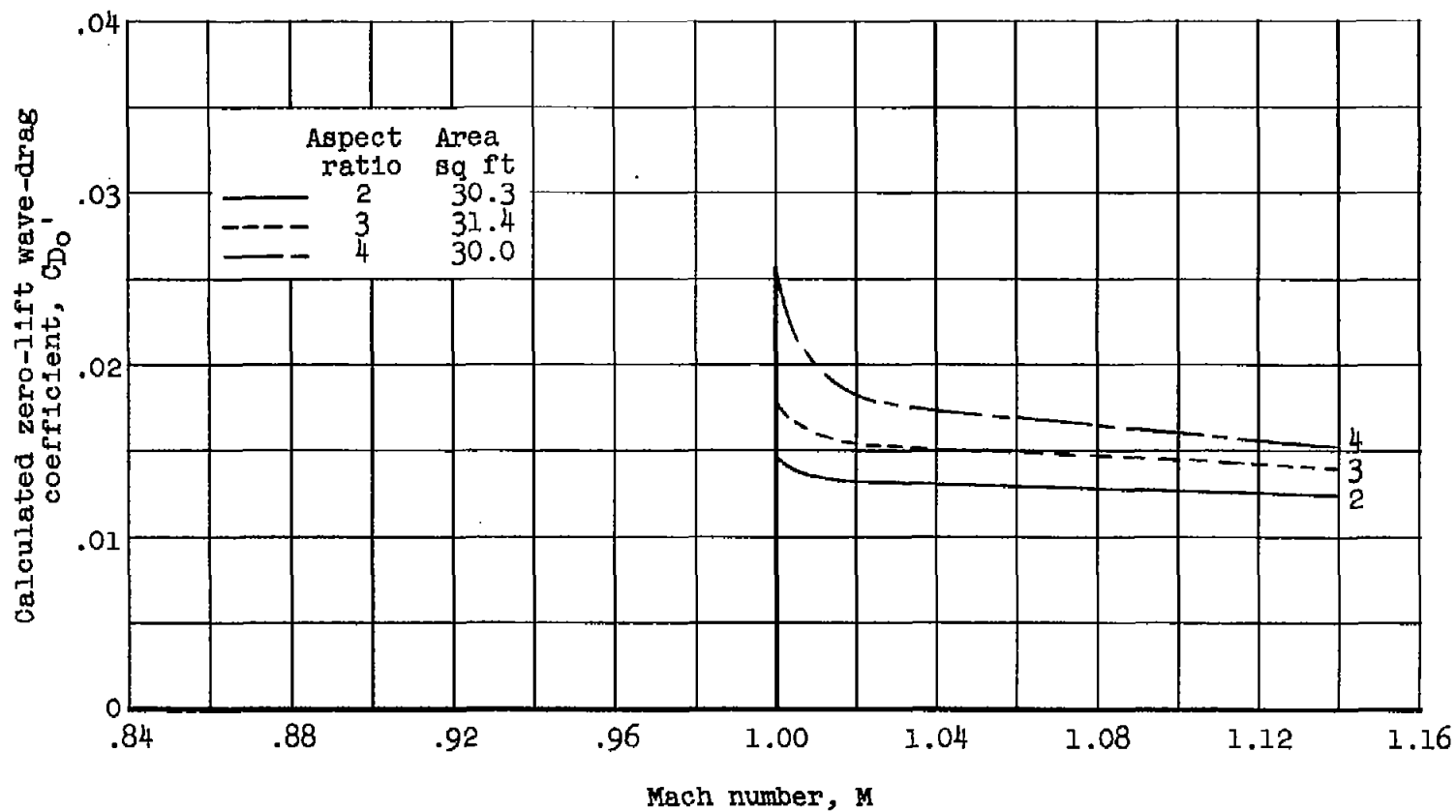
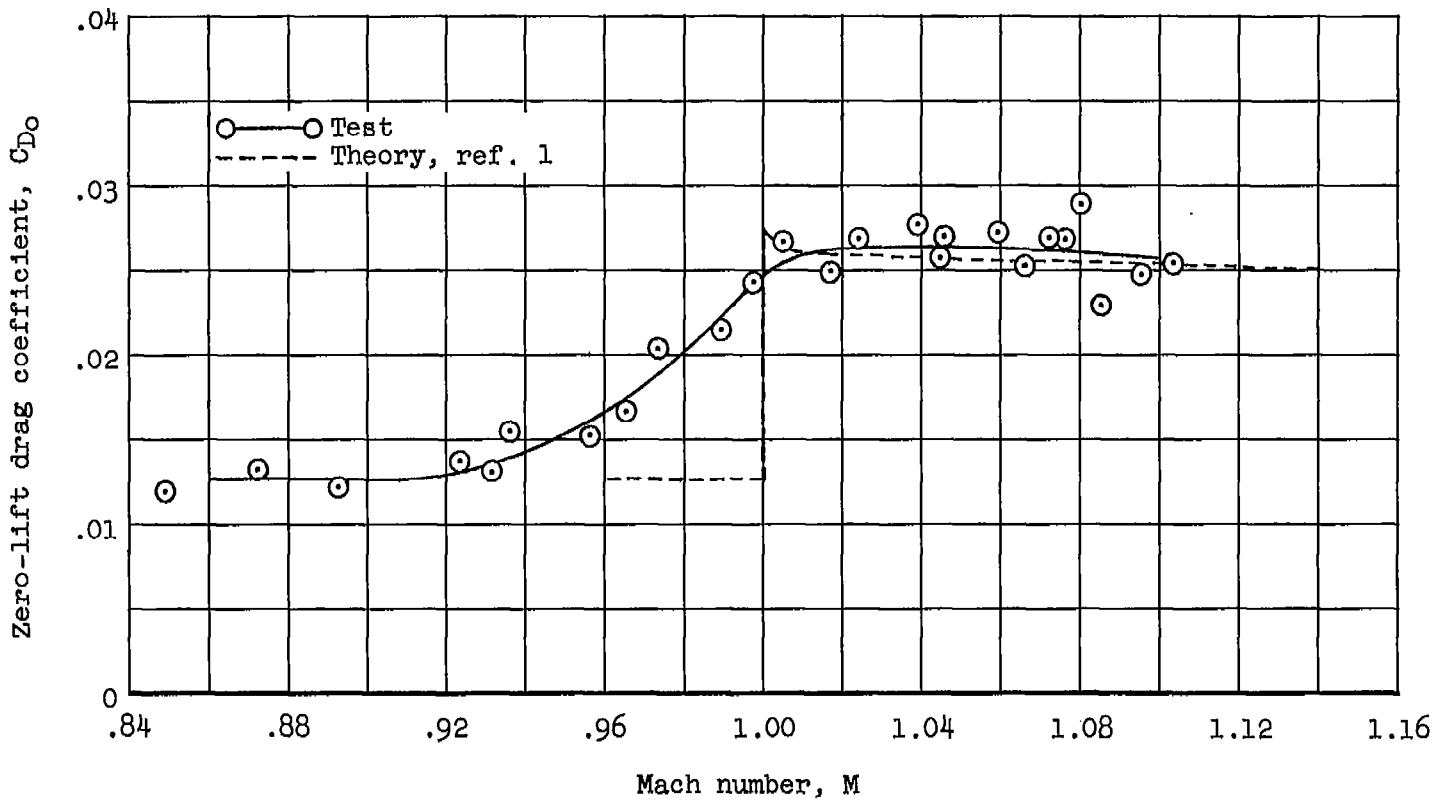
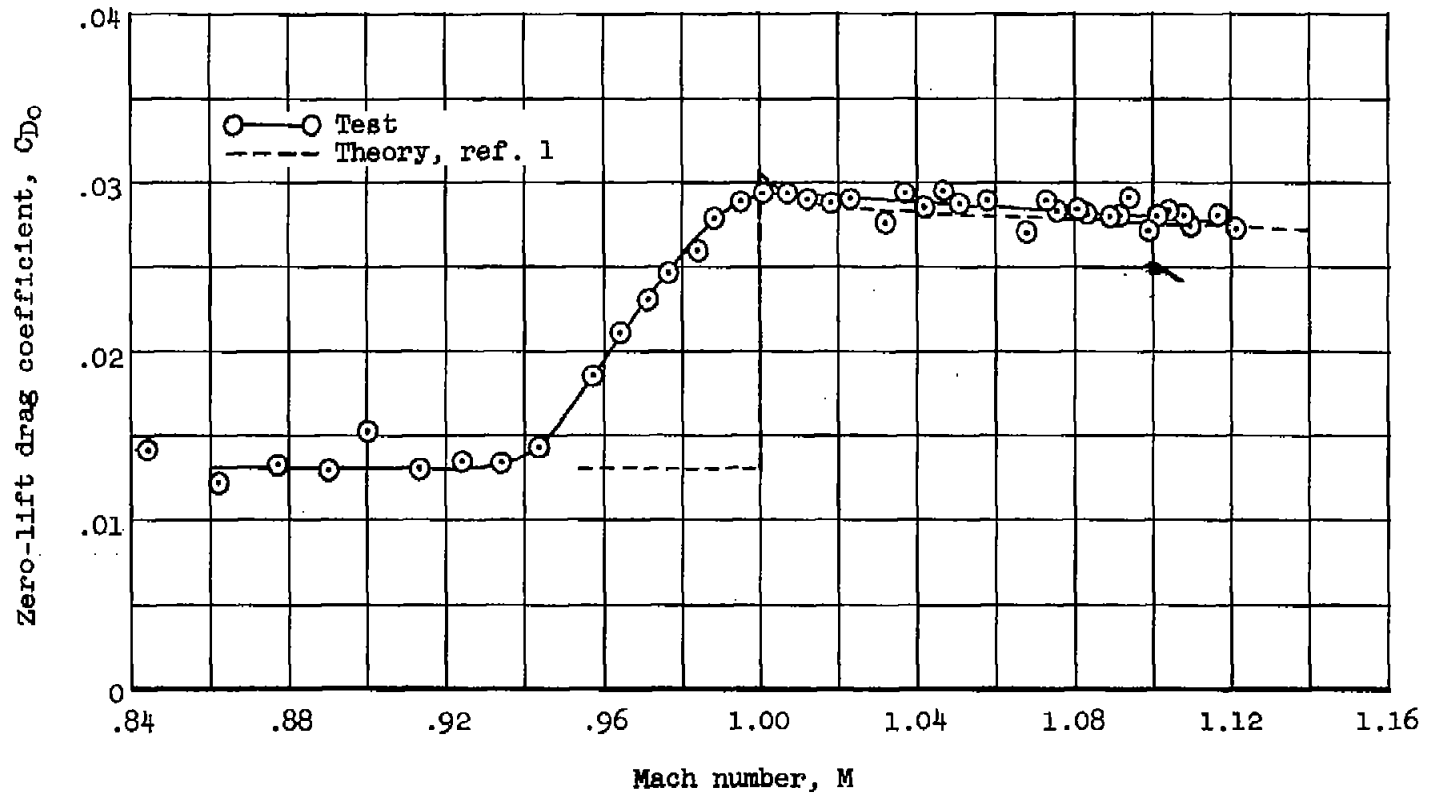


Figure 6.- Theoretical results for the triangular wings by the method of reference 1.



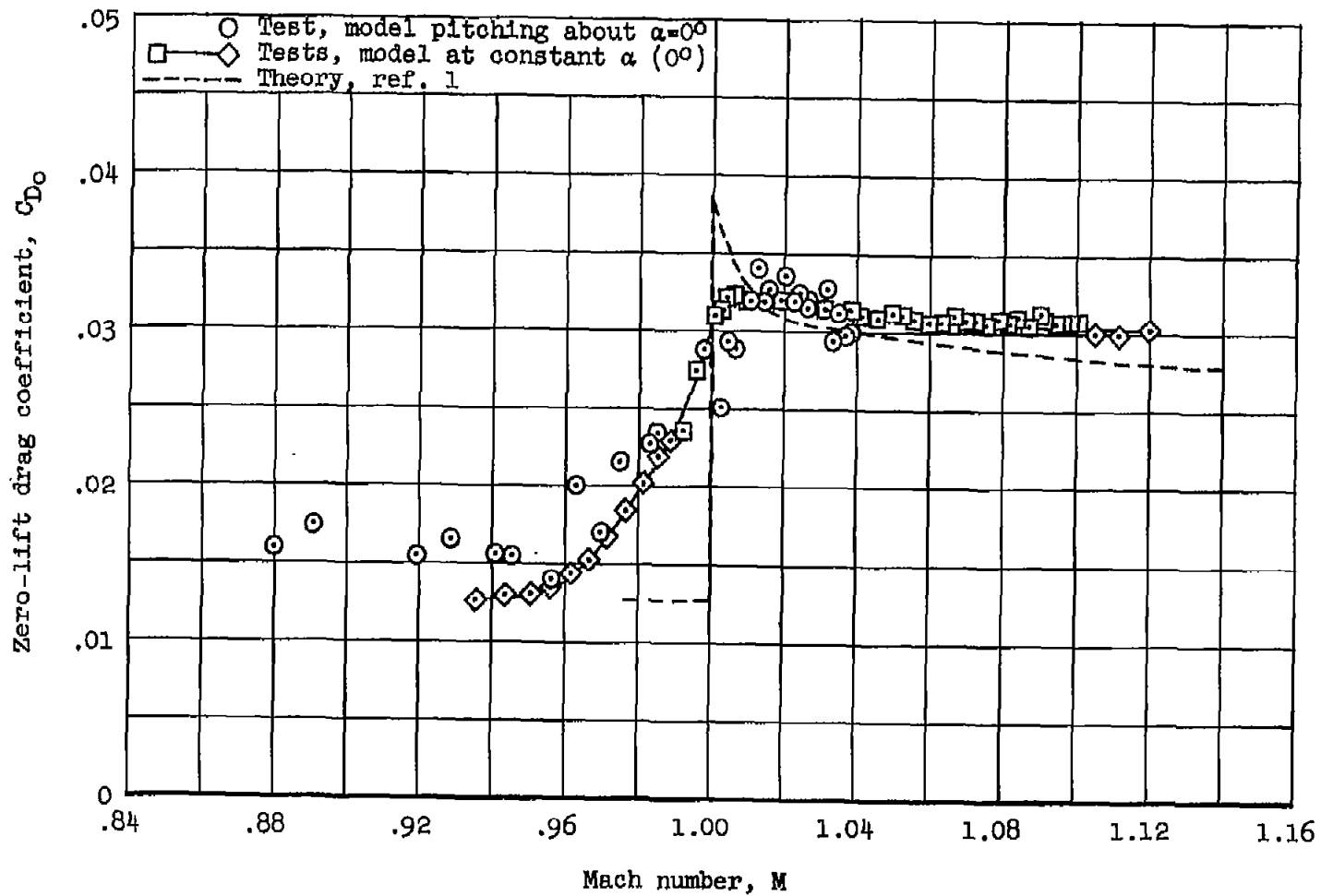
(a) Aspect-ratio-2 wing.

Figure 7.- Comparison of experimental zero-lift drag coefficients for each triangular wing with computed wave-drag coefficients added to the subsonic level of the experimental data.



(b) Aspect-ratio-3 wing.

Figure 7.- Continued.



(c) Aspect-ratio-4 wing.

Figure 7.- Concluded.

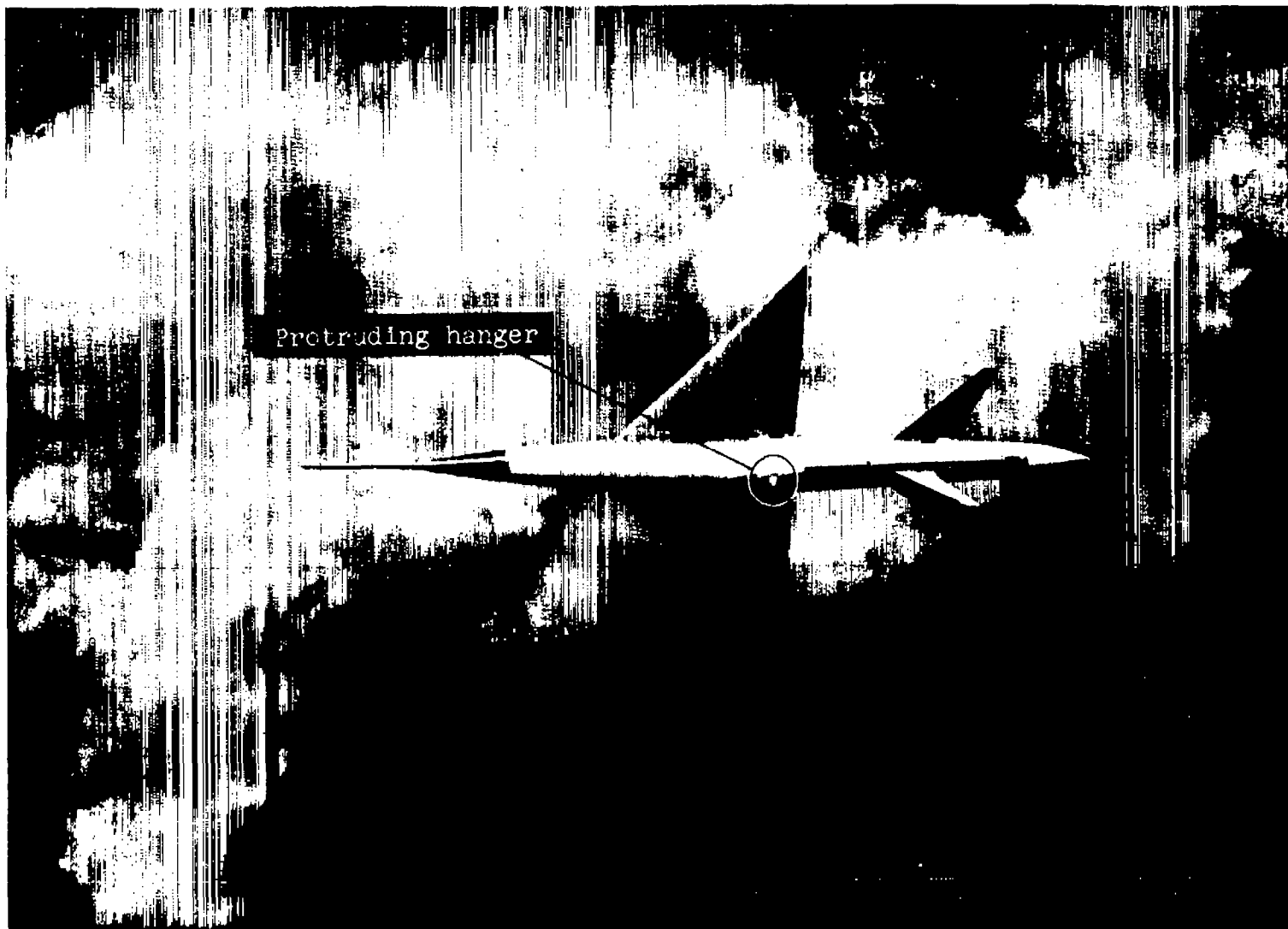


Figure 8.- Aspect-ratio-4 triangular-wing model in flight with protruding hanger.

A-17133.1

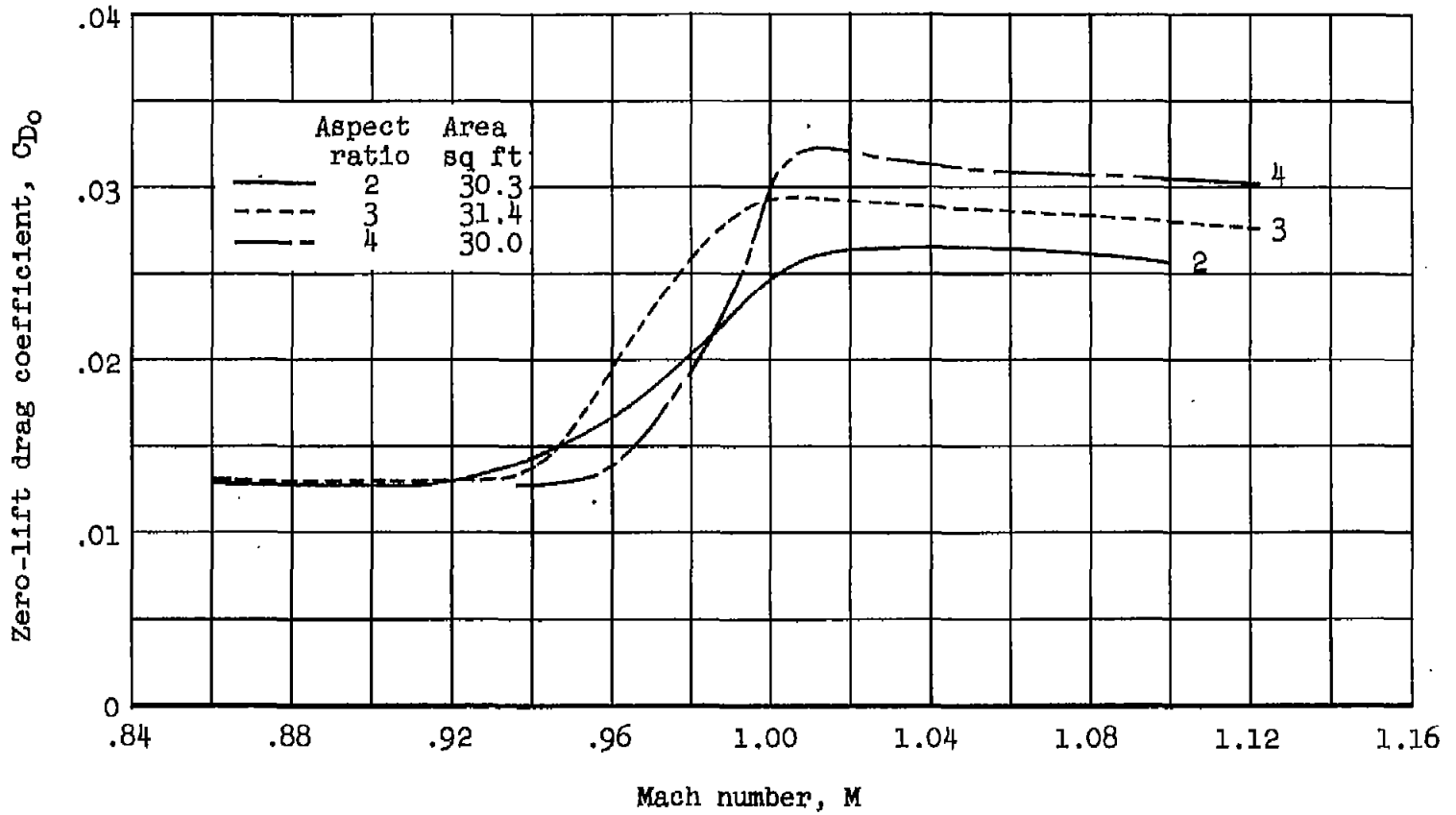
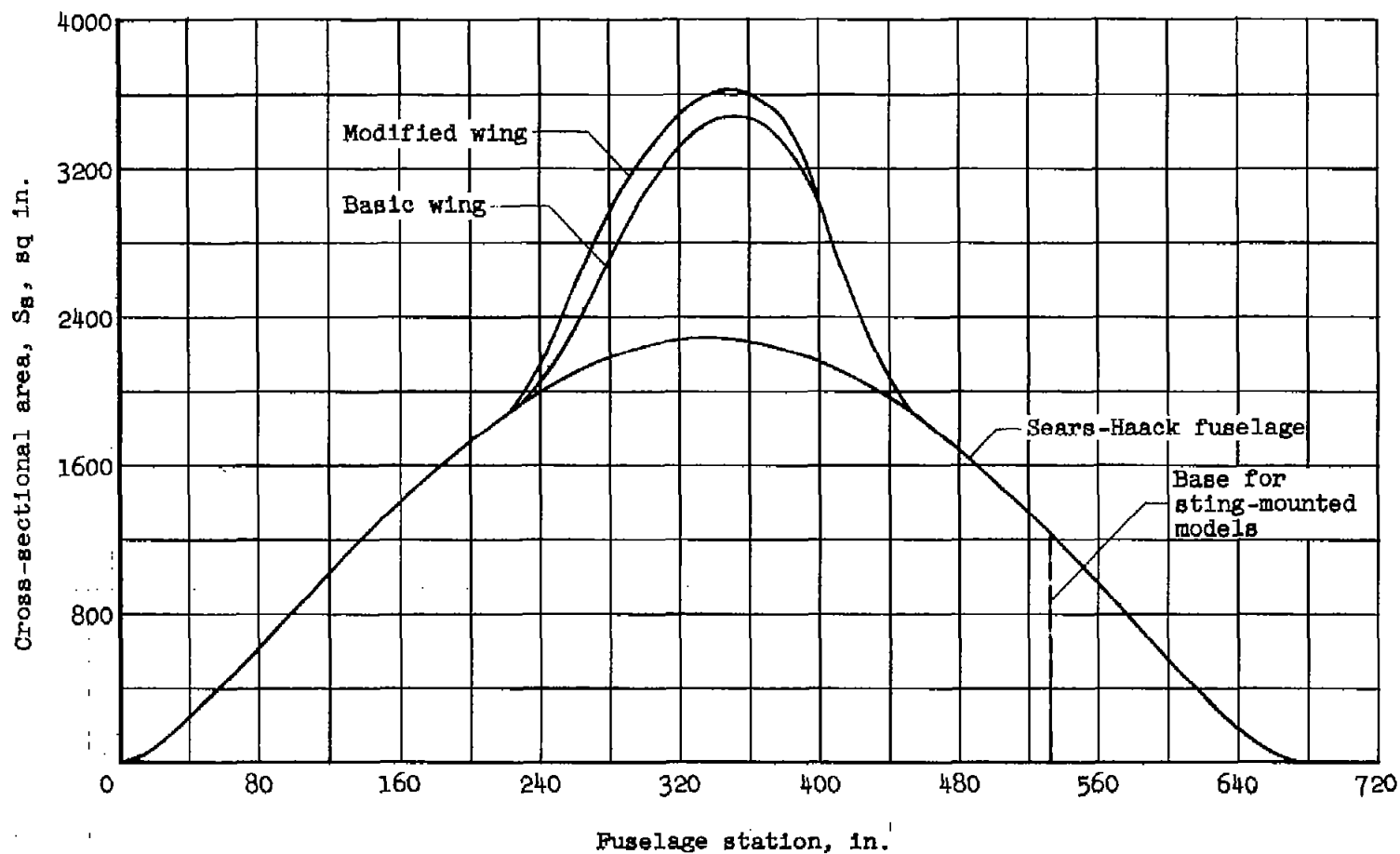
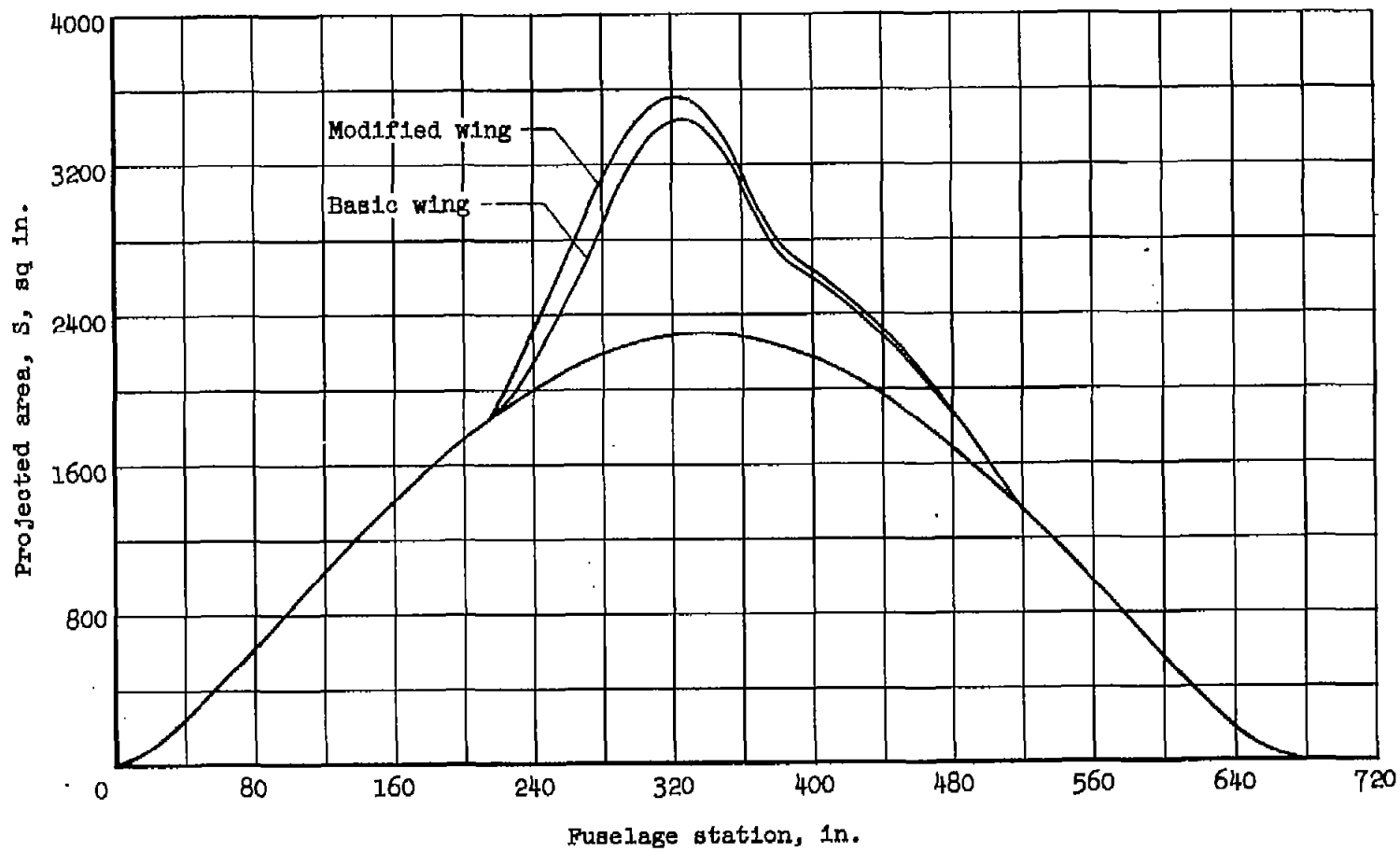


Figure 9.- Comparison of the experimental zero-lift drag coefficients for the triangular wings.



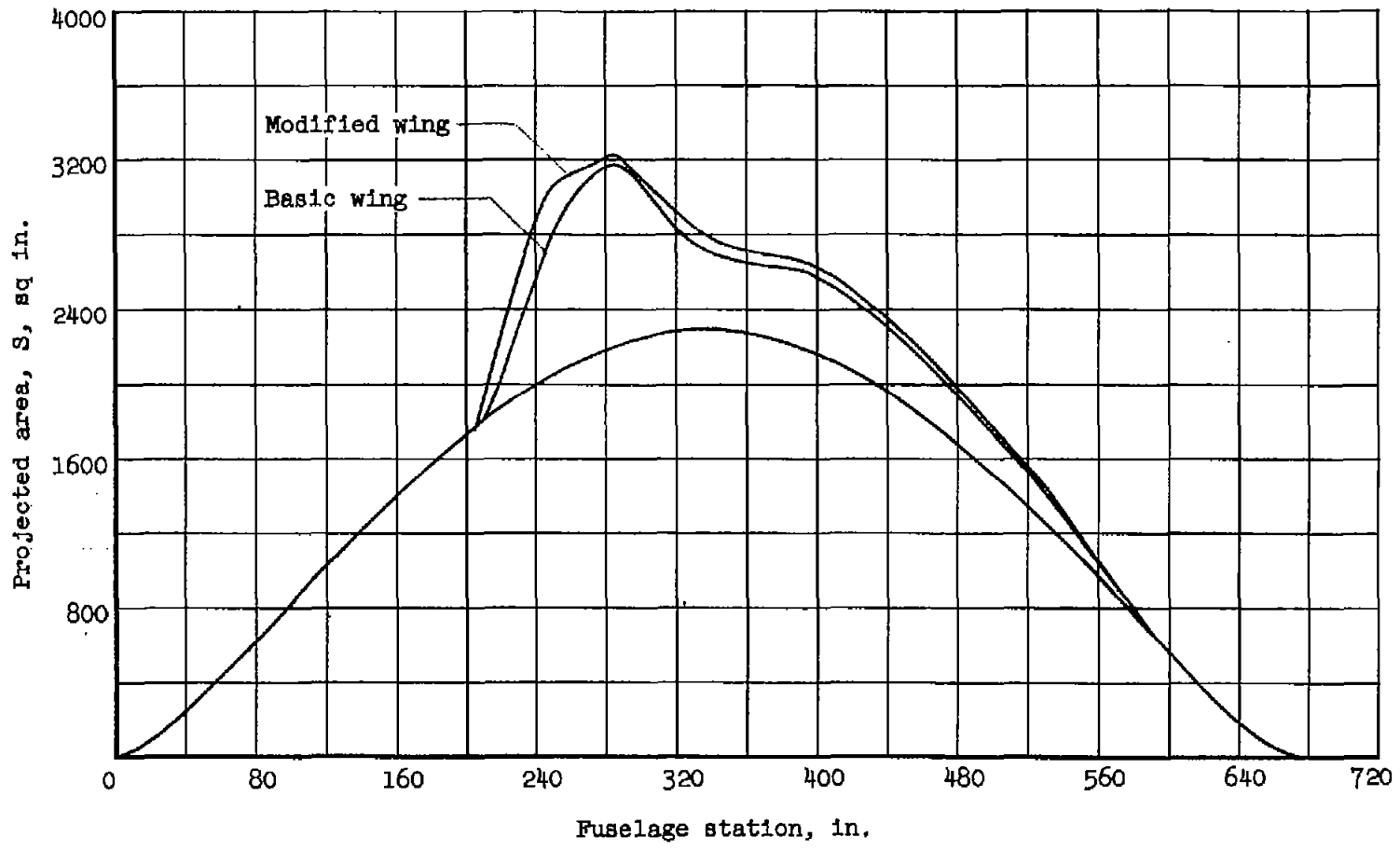
(a) $\theta=90^\circ$, $\psi=0^\circ$.

Figure 10.- Area distributions for the basic and modified swept-wing, full-scale models for a Mach number of 1.5.



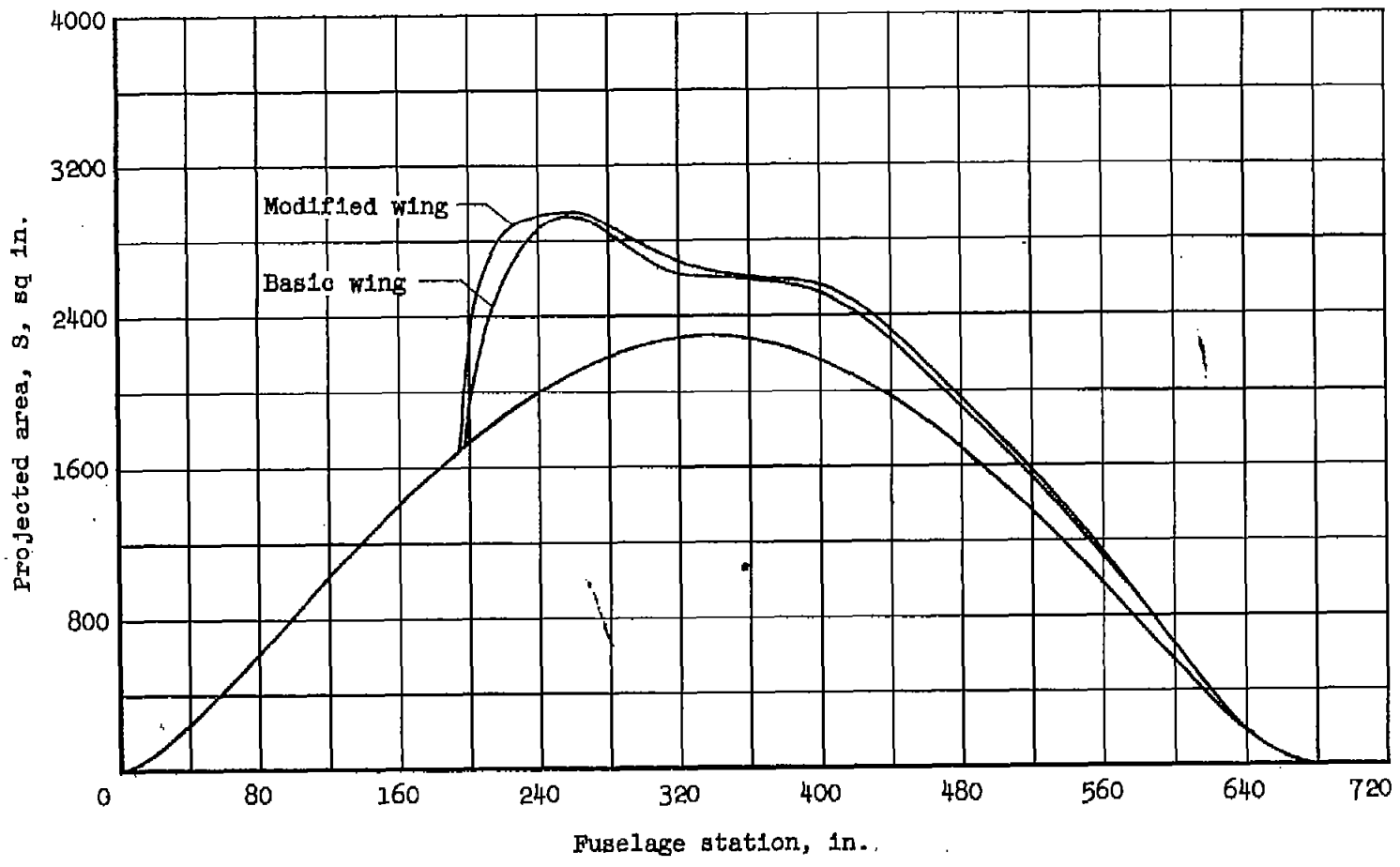
(b) $\theta=67.5^\circ$, $\psi=23.2^\circ$.

Figure 10.- Continued.



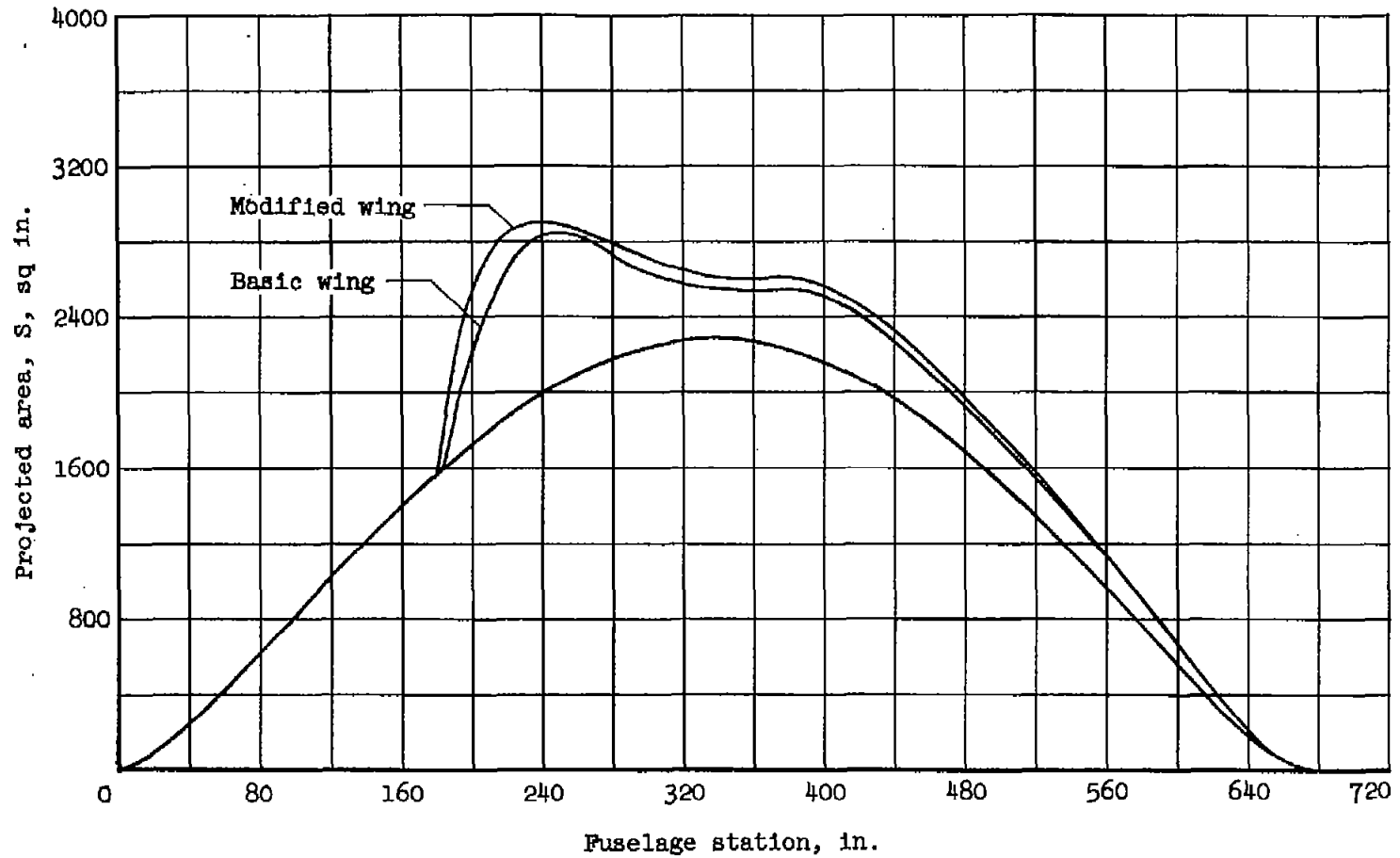
(c) $\theta=45^\circ$, $\psi=38.4^\circ$.

Figure 10.- Continued.



(d) $\theta=22.5^\circ$, $\psi=46.0^\circ$.

Figure 10.- Continued.



(e) $\theta=0^\circ$, $\psi=48.2^\circ$.

Figure 10.- Concluded.

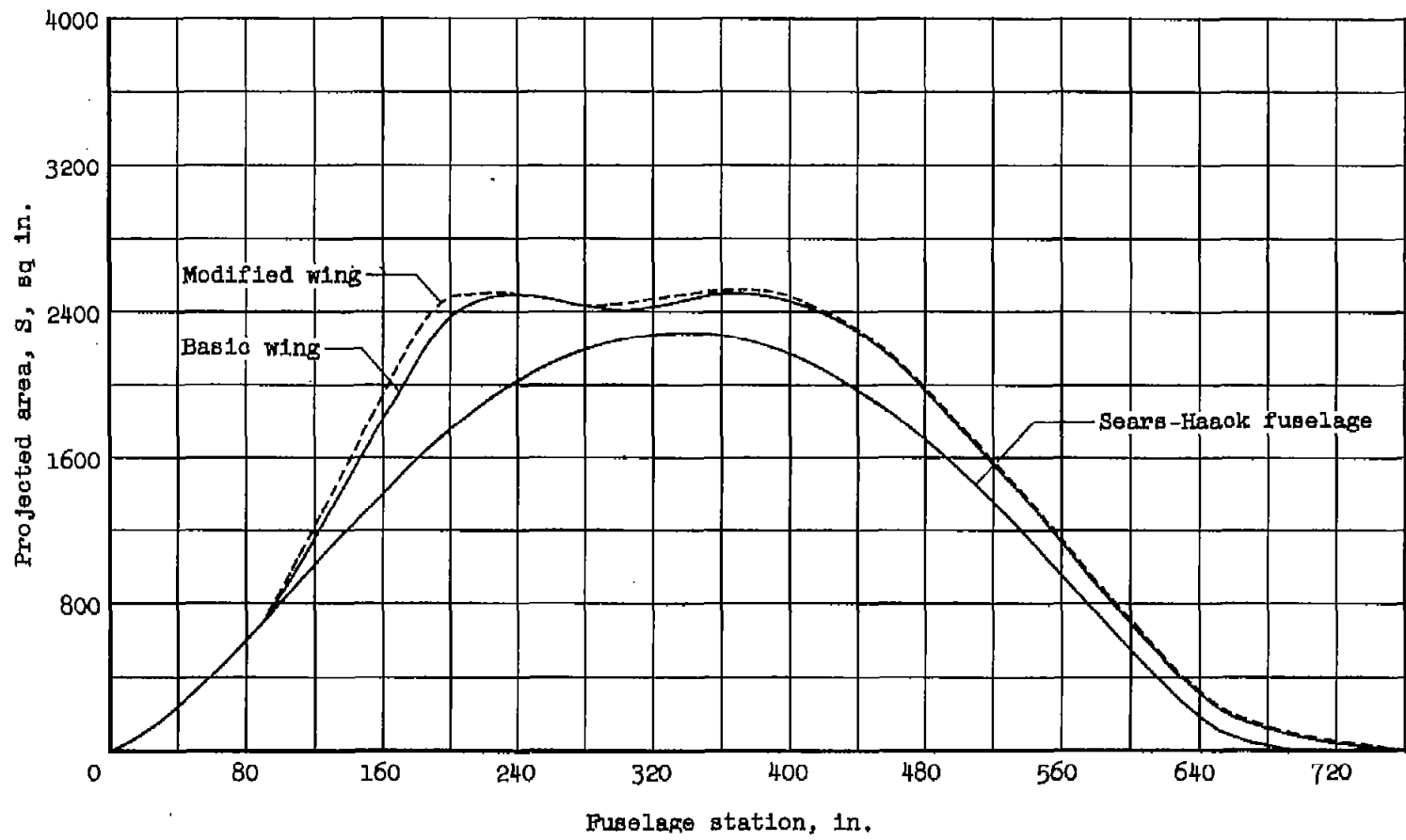
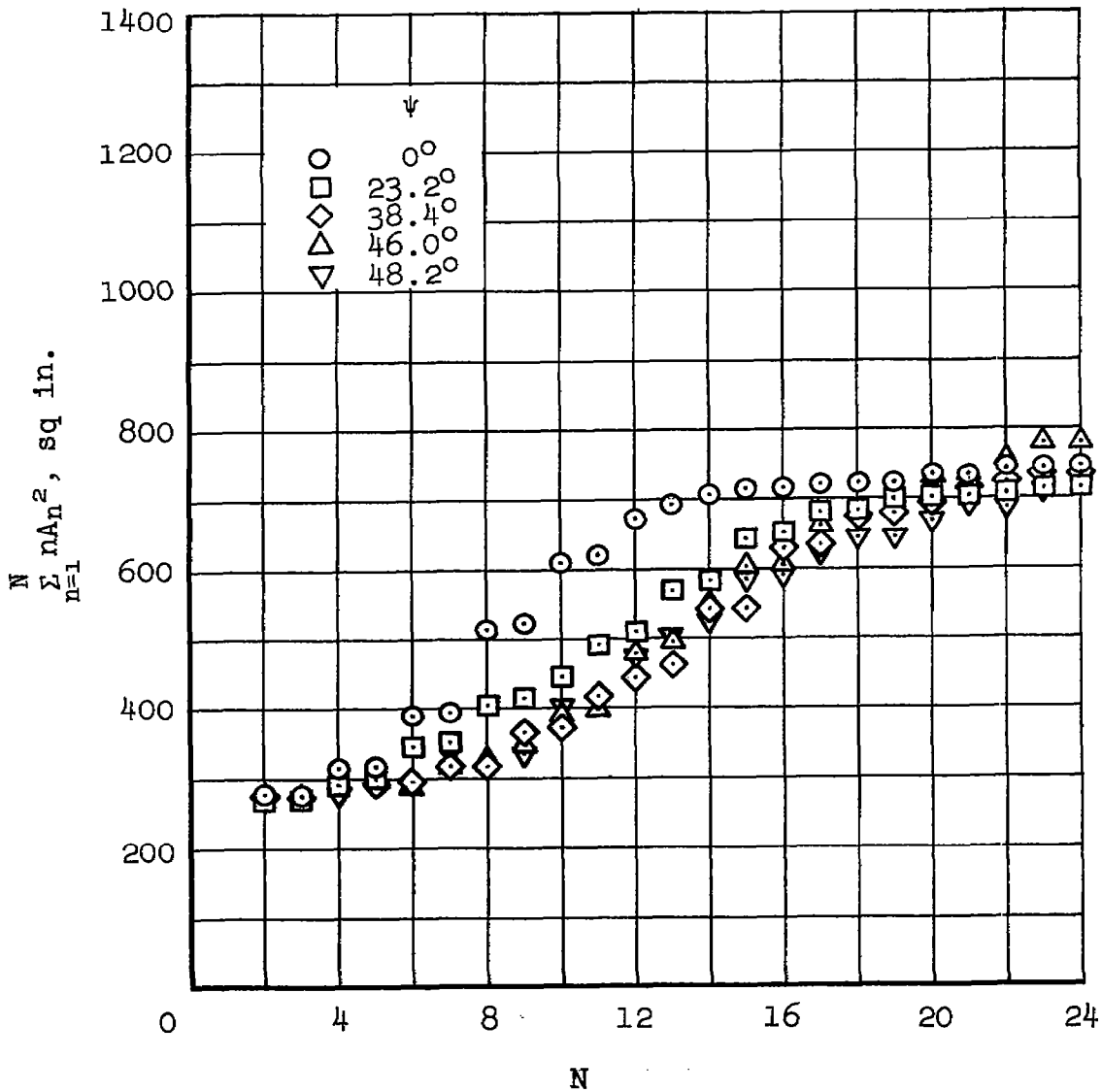
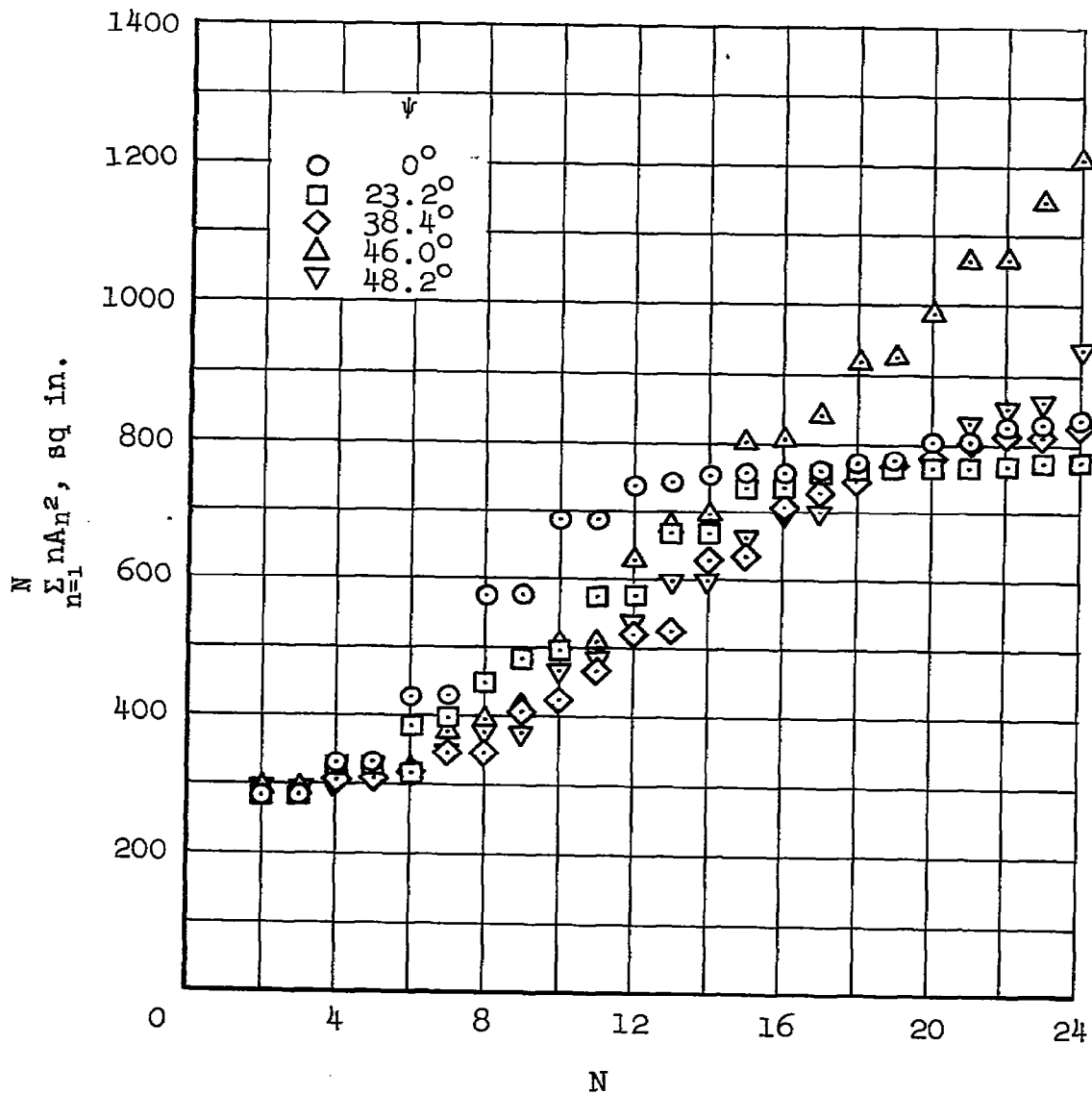


Figure 11.- Area distributions for the basic and modified swept-wing full-scale models for a Mach number of 1.9 ($\theta=0^\circ$, $\psi=58.25^\circ$).



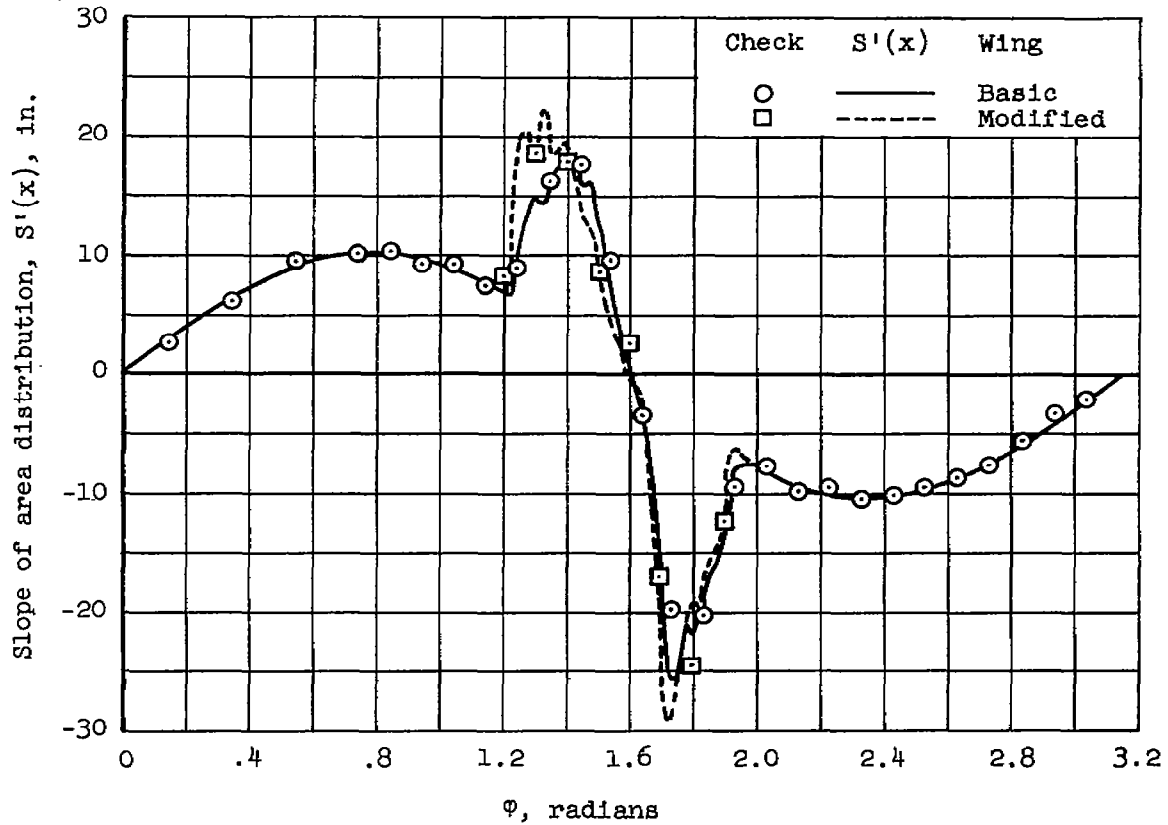
(a) Basic wing.

Figure 12.- Variation of $\sum_{n=1}^N n A_n^2$ with N for the swept-wing models for five cutting angles for a Mach number of 1.5.



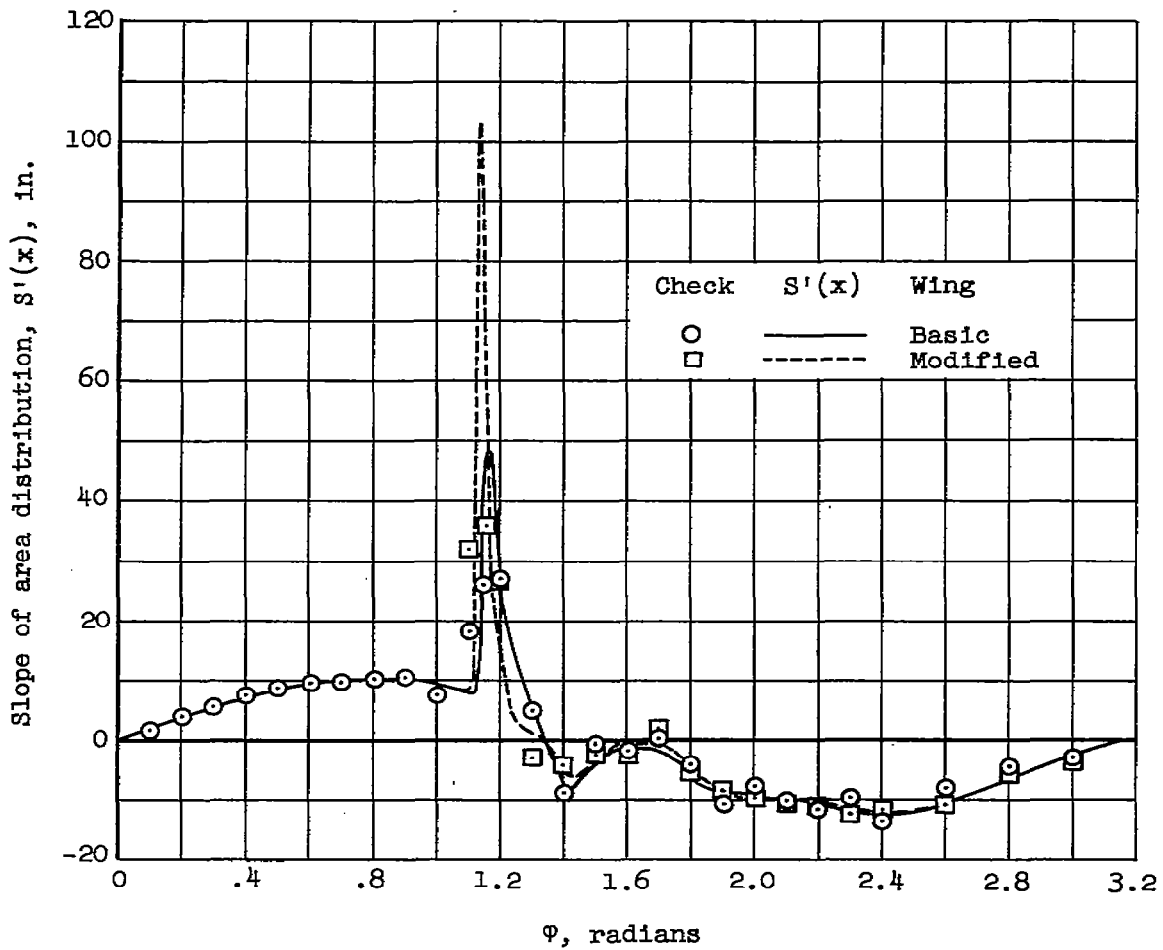
(b) Modified wing.

Figure 12.- Concluded.



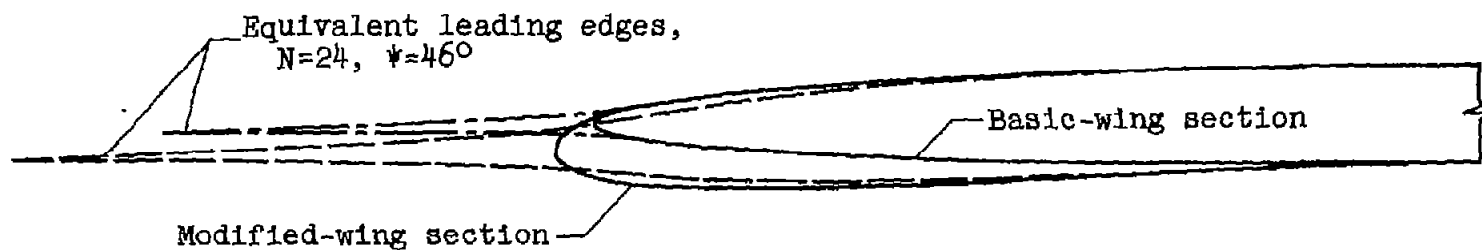
(a) $\theta=90^\circ$, $\psi=0^\circ$.

Figure 13.- Check of the effectiveness of the solution of the Fourier sine series (24 terms) to represent the curves of $S'(x)$ used in the wave-drag calculations for the swept-wing models.

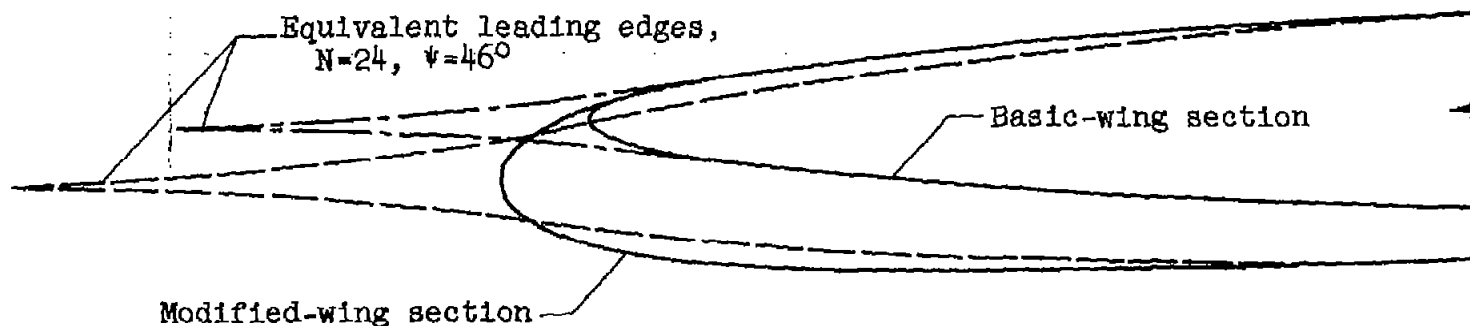


(b) $\theta=22.5^\circ$, $\psi=46.0^\circ$.

Figure 13.- Concluded.



(a) Wing-tip sections.



(b) Wing-root sections (spanwise station 26).

Figure 14.- Equivalent leading edges effectively added to the airfoil sections of the swept-wing models by wave-drag computations limited to 24 terms of a Fourier sine series (for $M > \sqrt{2}$).

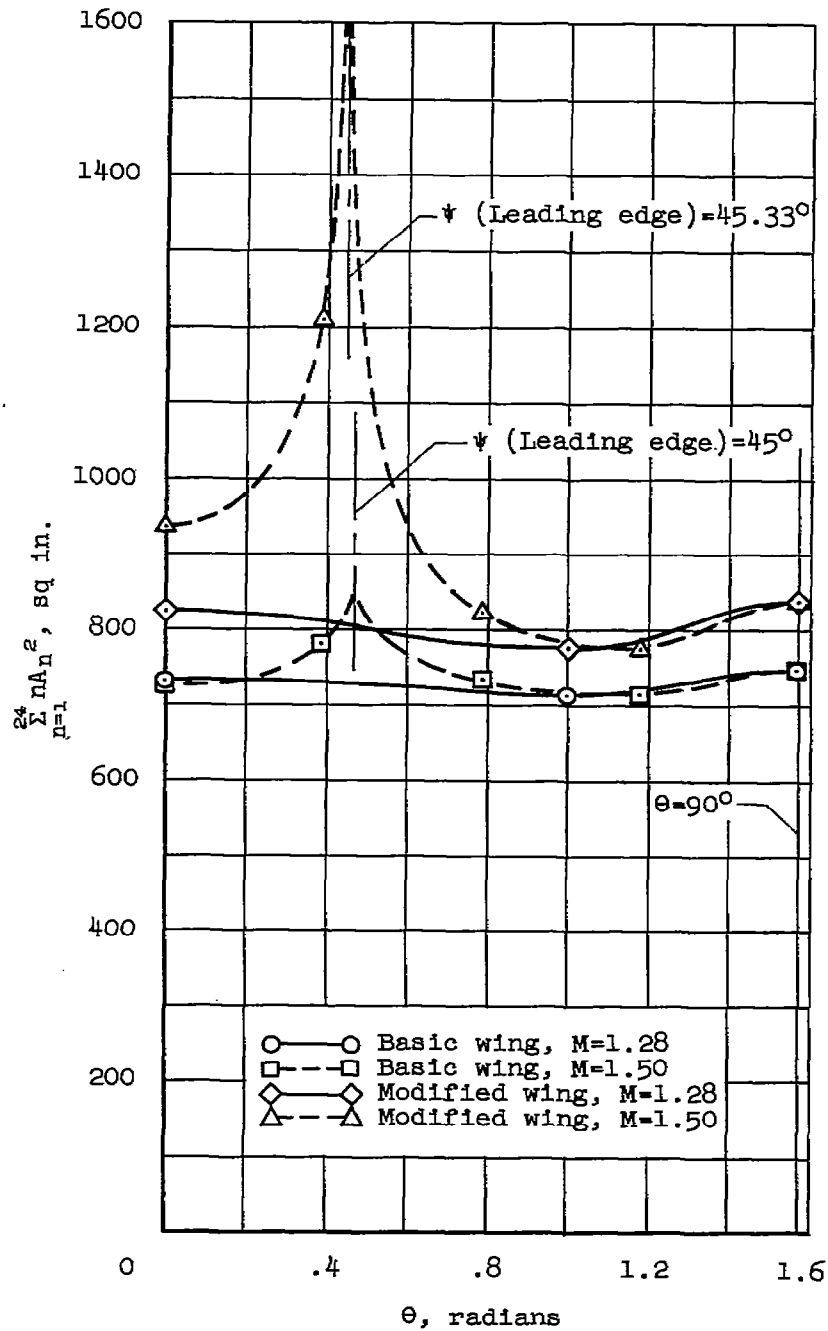


Figure 15.- Plot of the wave-drag parameter $\sum_{n=1}^{24} nA_n^2$ showing the peaks caused by cutting planes which are parallel to the wing leading edge.

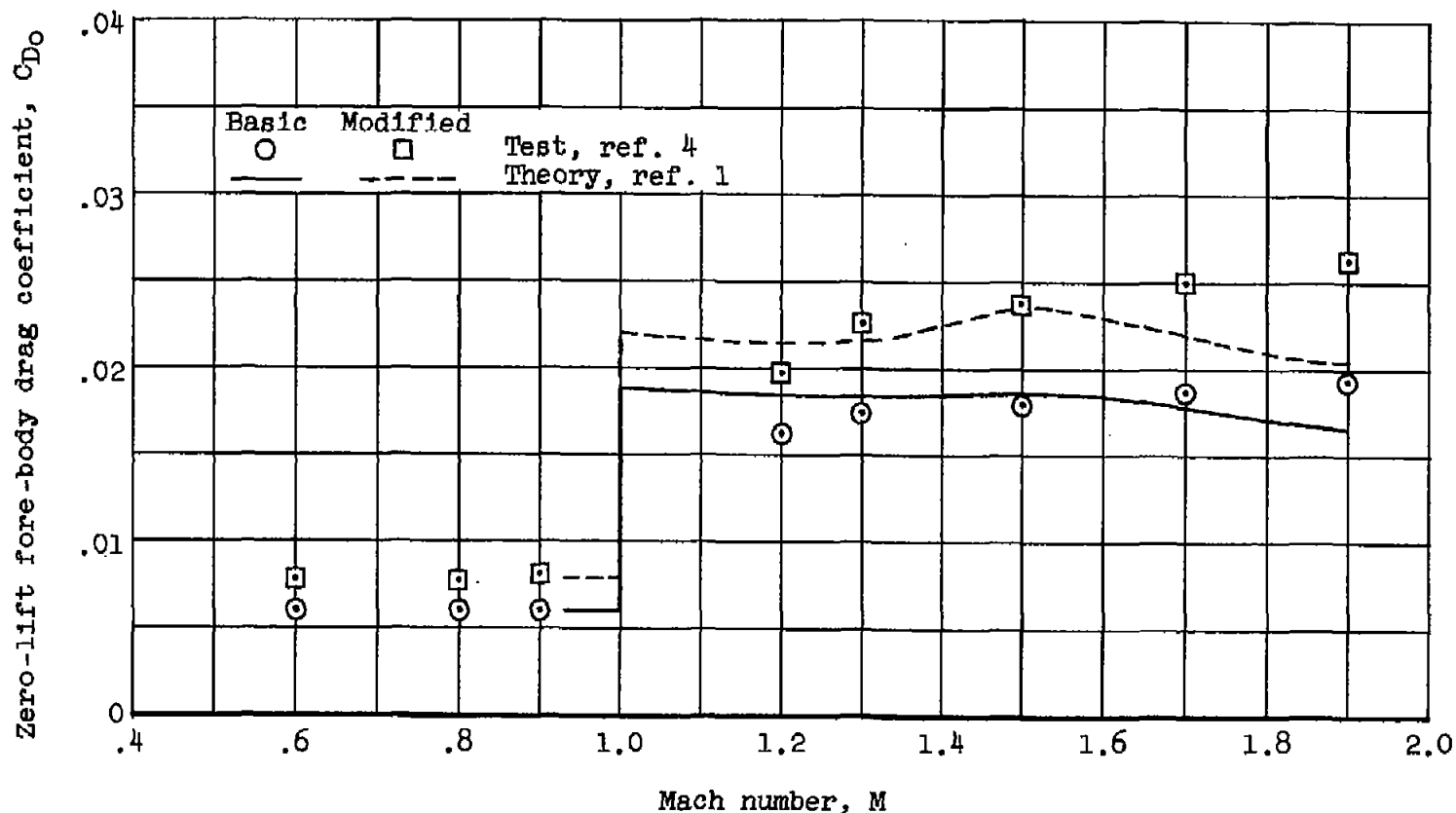


Figure 16.- Comparison of experimental zero-lift drag coefficients for the swept-wing tunnel models with computed wave-drag coefficients added to the subsonic level of the experimental data. Computed values above $M=\sqrt{2}$ are for the sharp nose sections of figure 14.

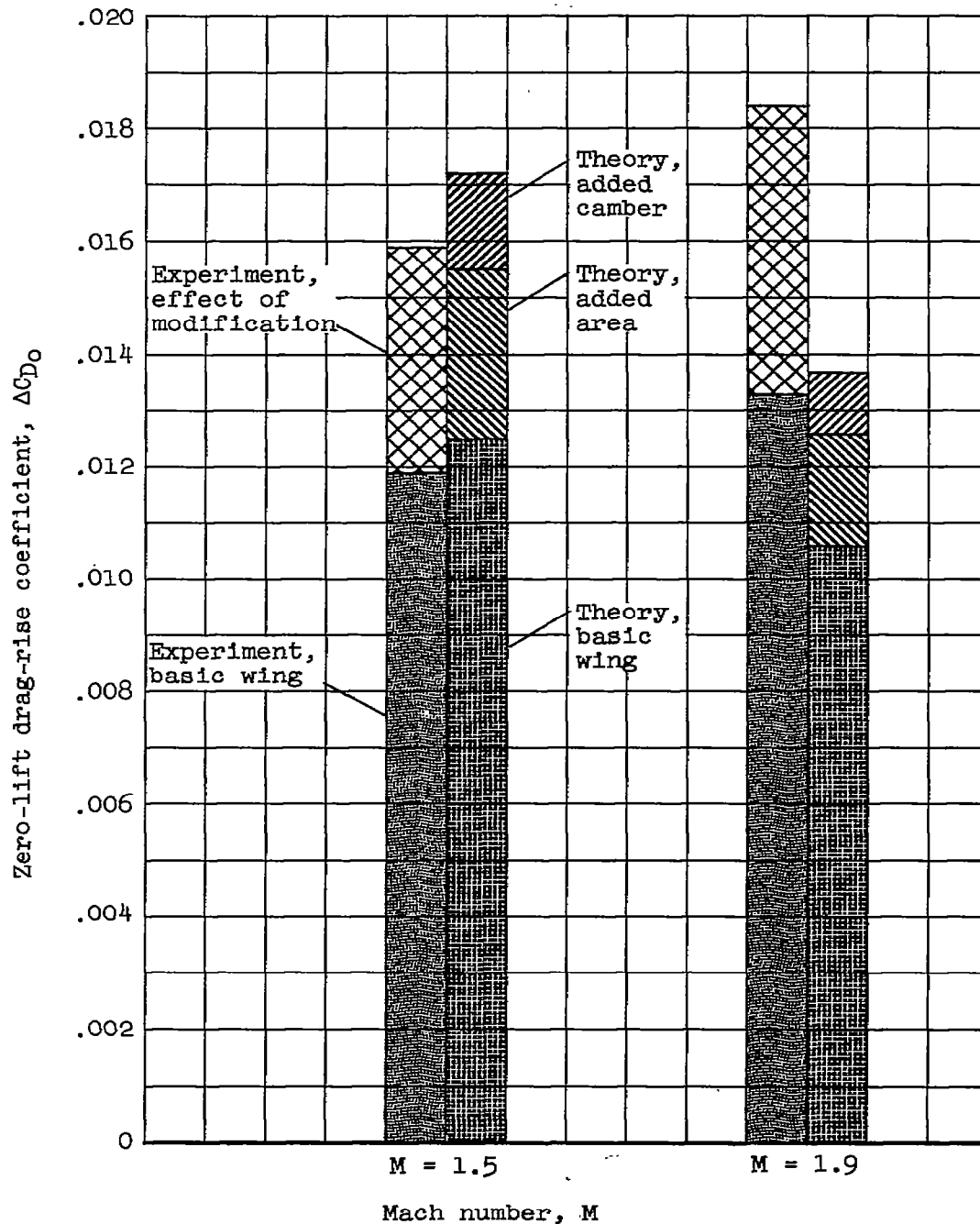


Figure 17.- Comparison at two Mach numbers of the experimental and theoretical zero-lift drag-rise coefficients of the basic and modified swept-wing models including a theoretical estimate of the effect of the added camber.



3 1176 01434 7497

